Volume 25
Number 25
7 July 2023
Pages 16659–17060

PCCP

Physical Chemistry Chemical Physics

rsc.li/pccp

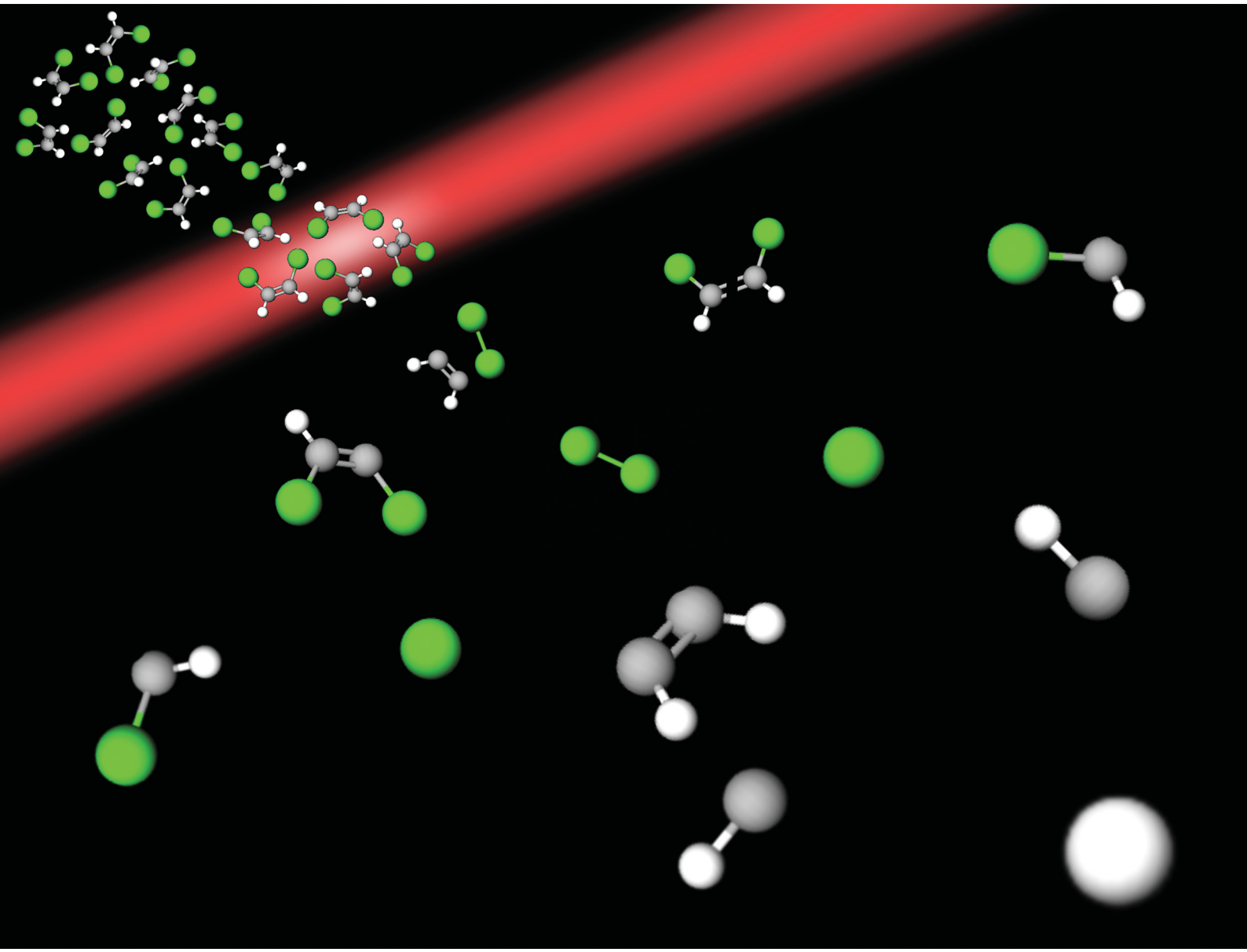

ISSN 1463-9076

ROYAL SOCIETY OF CHEMISTRY

PERSPECTIVE

Michael N. R. Ashfold *et al.*

Molecular photodissociation dynamics revealed by Coulomb explosion imaging

PCCP Owner Societies

PCCP

ROYAL SOCIETY OF CHEMISTRY

PERSPECTIVE

View Article Online
View Journal | View Issue

Cite this: *Phys. Chem. Chem. Phys.*, 2023, **25**, 16672

Molecular photodissociation dynamics revealed by Coulomb explosion imaging†

Stuart W. Crane, ‡[a] Jason W. L. Lee, [b] Michael N. R. Ashfold *[a] and Daniel Rolles [c]

Coulomb explosion imaging (CEI) methods are finding ever-growing use as a means of exploring and distinguishing the static stereo-configurations of small quantum systems (molecules, clusters, *etc*). CEI experiments initiated by ultrafast (femtosecond-duration) laser pulses also allow opportunities to track the time-evolution of molecular structures, and thereby advance understanding of molecular fragmentation processes. This Perspective illustrates two emerging families of dynamical studies. 'One-colour' studies (employing strong field ionisation driven by intense near infrared or single X-ray or extreme ultraviolet laser pulses) afford routes to preparing multiply charged molecular cations and exploring how their fragmentation progresses from valence-dominated to Coulomb-dominated dynamics with increasing charge and how this evolution varies with molecular size and composition. 'Two-colour' studies use one ultrashort laser pulse to create electronically excited neutral molecules (or monocations), whose structural evolution is then probed as a function of pump–probe delay using an ultrafast ionisation pulse along with time and position-sensitive detection methods. This latter type of experiment has the potential to return new insights into not just molecular fragmentation processes but also charge transfer processes between moieties separating with much better defined stereochemical control than in contemporary ion-atom and ion-molecule charge transfer studies.

Received 17th April 2023,
Accepted 1st June 2023

DOI: 10.1039/d3cp01740k

rsc.li/pccp

[a] *School of Chemistry, University of Bristol, Bristol, BS8 1TS, UK. E-mail: mike.ashfold@bristol.ac.uk*
[b] *Department of Chemistry, University of Oxford, Oxford, OX1 3TA, UK*
[c] *J.R. Macdonald Laboratory, Department of Physics, Kansas State University, Manhattan, KS 66506, USA*

† Electronic supplementary information (ESI) available. See DOI: https://doi.org/10.1039/d3cp01740k

‡ Current address: Department of Chemistry, Brown University, Providence, RI 02912, USA.

I. Introduction

Photodissociation is a particular form of chemical reaction in which the absorption of a photon (or multiple photons) of light by a molecule leads to its fragmentation. Vital examples include the photodissociation of oxygen molecules (O_2) to oxygen (O) atoms, driven by the absorption of short wavelength photons at

Stuart W. Crane

Stuart W. Crane graduated from Heriot-Watt University with a Masters degree in Physics (MPhys) in 2014, and subsequently obtained his PhD from the same institution in 2018. Following postdoctoral research positions at the University of Bristol (2018–2020) and Heriot-Watt University (2021–2022), Stuart is presently a research associate in the Weber Research Lab at Brown University. His research interests include ultrafast molecular photochemistry and gas-phase spectroscopy.

Jason W. L. Lee

Jason W. L. Lee graduated from the University of Cambridge with a Bachelor's degree and Masters in Natural Sciences (Physical) in 2010, followed by a DPhil in Physical and Theoretical Chemistry from the University of Oxford in 2014. He continued at the University of Oxford as a postdoc before joining the Photon Science – Spectroscopy of Molecular Processes (FS-SMP) group at the Deutsches Elektronen-Synchrotron (DESY), Hamburg in 2019. His research focusses on the development and application of novel imaging methods and technology to explore gas phase molecular dynamics.

high altitudes in the Earth's atmosphere, and of ozone (O_3) to O_2 plus an O atom by longer wavelength ultraviolet (UV) photons lower in the stratosphere. Together, these two photodissociation processes are key to establishing the localisation (in altitude) of the ozone layer.[1,2]

Those interested in molecular photodissociation dynamics seek insights and understanding beyond simply determining the photoproducts. Such studies are often conducted as 'pump–probe' experiments, in the gas phase, at low pressures, mostly under jet-cooled molecular beam (*i.e.* collision-free) conditions, and seek to answer questions like: in what quantum (electronic, vibrational, rotational, spin–orbit, *etc.*) states are the products formed, and/or what are the various product recoil velocities, $\boldsymbol{v}$? The photoexcitation event usually involves an electric dipole transition, the probability of which is maximised when the electric ($\boldsymbol{\varepsilon}$) vector of the exciting radiation is aligned parallel to the transition dipole moment ($\boldsymbol{\mu}$). Thus, photoexcitation typically creates an anisotropic distribution of excited molecules. If the photoexcited molecules dissociate rapidly (*i.e.* on a timescale that is fast compared with the period of molecular rotation), this spatial anisotropy should be revealed as an angular anisotropy in the product yield, *i.e.* in a correlation between $\boldsymbol{\mu}$ and $\boldsymbol{v}$, and thus between $\boldsymbol{\varepsilon}$ and $\boldsymbol{v}$. Other correlations, *e.g.* between $\boldsymbol{\mu}$ and the rotational angular momentum, $\boldsymbol{J}$, of a photofragment, and even between the fragment $\boldsymbol{v}$ and $\boldsymbol{J}$ vectors, can be observed in favourable cases.[3] All such information reports on the forces acting on the nuclei of the molecule in the act of dissociating. These forces are determined by the topography of the potential energy surface(s) (PES(s)) sampled during the dissociation process. Calculations of excited (and ground) state PESs for small and medium-sized neutral molecules, and of the non-adiabatic couplings between these PESs, are now amenable to contemporary *ab initio* electronic structure methods. Methods of calculating nuclear dynamics on such PESs are also advancing impressively, enabling increasingly rigorous and fruitful points of comparison between experiment and theory.[4–7]

Until quite recently, experimental studies of molecular photofragmentation processes in the gas phase have tended to group into one of two classes.[8] Both start with the 'pump' step – photoexcitation, typically with a short duration pulse of reasonably monochromatic light from a laser. One class relies on 'probing' the (typically electronic) spectrum of one or more of the photofragments – which in this class of experiments are most usually diatomic species. The density of photofragments in such experiments is generally too low to allow use of absorption detection methods; favoured probe methods include laser induced fluorescence (LIF) and resonance enhanced multiphoton ionisation (REMPI) spectroscopy. Given a thorough understanding of the diatomic fragment spectroscopy, analysis of the spectral line intensities allows determination of the product quantum state population distributions,[9] while measurements of Doppler broadened spectral lineshapes (linewidths) can give information about the fragment recoil velocities.[10]

The second class of experiments report directly on the velocities (and thus the translational energies) of one or more of the photofragments. Early photofragment translational spectroscopy (PTS) experiments used electron impact ionisation and mass spectrometric detection methods after the photofragments had recoiled along the detection axis. Current methods of choice 'tag' the fragment of interest immediately after its creation. Velocity map imaging (VMI) methods (Fig. 1) where the target photofragment is ionised at source (in a state-selective manner, by REMPI) and then accelerated onto a two-dimensional (2-D) time and position-sensitive detector, have had major impact in this field.[11–15] The image reports the velocity distribution of the probed fragment and, in favourable cases, shows structure which upon analysis reveals the quantum state population distribution in the partner fragment. A variant, that has been widely applied in studies of the photodissociation of hydride molecules that yield H

Michael N. R. Ashfold

Michael N. R. Ashfold obtained his PhD from the University of Birmingham in 1978. After postdoctoral research at Oxford, he was appointed to a Lectureship at the University of Bristol, where he was promoted to a Chair in Physical Chemistry in 1992. He retired from the Leverhulme Chair of Chemistry in late 2020 and is now an Emeritus Professor at Bristol. He was elected to the Fellowship of the Royal Society in 2009 and is a past winner of the Corday-Morgan, Tilden and Liversidge Prizes of the Royal Society of Chemistry. His research interests include gas phase molecular photochemistry and spectroscopy.

Daniel Rolles

Daniel Rolles obtained his PhD from the Technical University Berlin in 2005 for research performed at the Fritz Haber Institute and Lawrence Berkeley Laboratory. After postdoctoral research in Berkeley, he joined the Max Planck Advanced Study Group at the Center for Free-Electron Laser Science in Hamburg in 2008. Subsequently, he led a Helmholtz junior research group at DESY before being appointed as an Assistant Professor in Physics at the J. R. Macdonald Laboratory at Kansas State University in 2015 and promoted to Associate Professor in 2020. His research interests include ultrafast atomic and molecular physics and gas-phase photochemistry experiments.

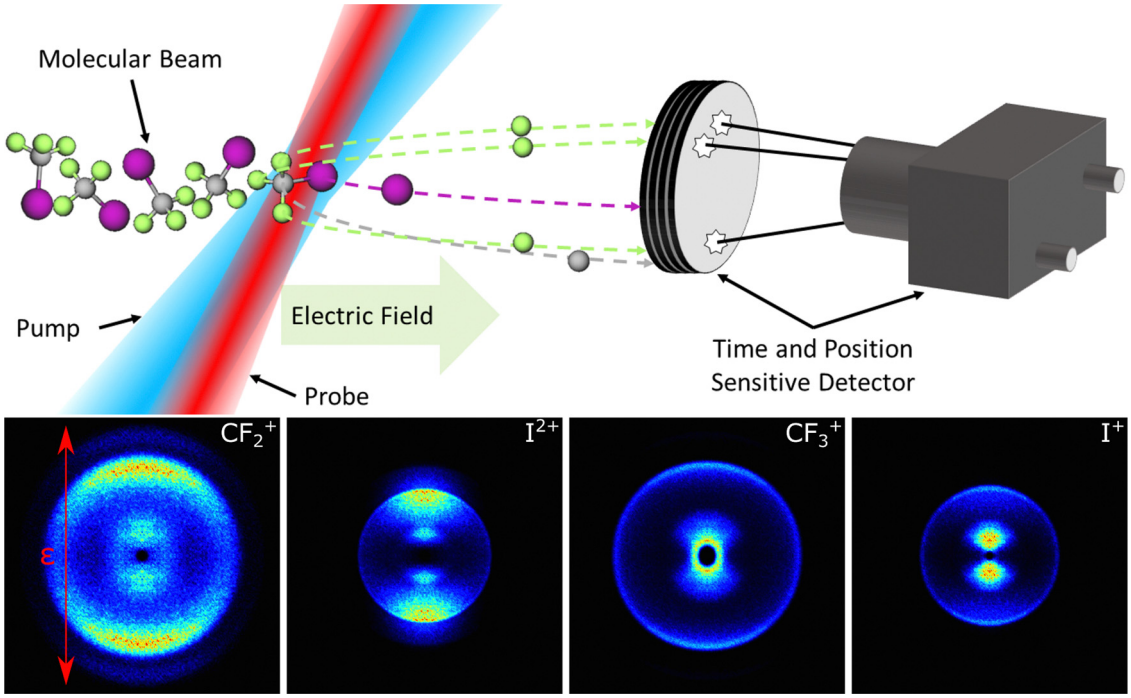

Fig. 1 (a) Schematic of a velocity-map imaging (VMI) experiment. A molecular beam of the target molecule (usually seeded in excess inert carrier gas) is crossed with a pump laser pulse, which initiates photodissociation. One (or more) chosen fragments are then ionised, using an appropriate probe laser pulse, and the charged atomic and/or molecular fragments are accelerated towards a position-sensitive detector by an electric field, yielding an (*x*, *y*, *t*) data point for each fragment ion. The ion arrival times correlate with their mass-to-charge (*m*/*z*) ratio, and the arrival positions correlate with their velocities. VMI studies of near infrared (NIR) strong field ionisation (SFI) or extreme UV (XUV) induced Coulomb explosions such as those described in Section II employ a similar set-up but with just one ultrafast laser pulse to induce CE. VMI studies of molecular photofragmentation processes using CE as the probe, such as those described in Section III, use ultrafast NIR SFI or XUV photons as the probe pulse. (b) Illustrative velocity map images of CF_2^+, I^{2+}, CF_3^+ and I^+ fragment ions from NIR SFI of CF_3I at I = 650 TW cm^{-2}.

(or D) atom fragments, involves two photon resonant excitation to Rydberg states of the H (D) atom lying at energies just below the ionisation limit.[16] These Rydberg states are sufficiently long lived to allow measurement of their times-of-arrival at a distant detector. Such 'Rydberg tagging' experiments also return velocity information, *i.e.* the fragment recoil speeds and directions. Combining such data with the requirements of momentum and total energy conservation in the overall photodissociation process can yield parent bond dissociation energies and detailed insights into the partitioning of any excess energy (*i.e.* energy provided by the pump photon in excess of that required to break the bond) within the products and thus the photodissociation dynamics.[17,18] Again, however, the data returned by the probe process generally requires quite detailed knowledge and understanding of the spectroscopy of the partner fragment.

The introduction of femtosecond lasers as a mainstream laboratory tool saw the growth of an alternative family of pump–probe experiments offering much higher time resolution but, in many cases, lower spectral resolution. The focus now turned to exploring molecular photodissociation dynamics by probing the evolution from excited parent molecule to dissociation products in real time, rather than interrogating the asymptotic fragments in the greatest possible detail.[19] The first such experiments typically used gas phase samples and LIF or REMPI (*i.e.* spectroscopy based) probe methods, but interest was growing in the use of other probe techniques like time-resolved photoelectron spectroscopy[20–24] and techniques with the potential to yield structural information directly. Other ultrafast pump–probe studies have sought to explore the dynamical aspects of molecular photofragmentation processes in solution. Transient absorption probe methods offer a means of tracking the formation (and subsequent relaxation) of not just 'traditional' photofragments formed by bond fission,[25–27] but also of acyclic isomers formed by photoinduced bond fission in a cyclic parent molecule.[28]

Returning to the gas phase, ultrafast electron diffraction probe methods attracted early attention,[29] but achieving sufficiently intense, short duration electron pulses to enable measurable signals from dilute gas phase samples is a major challenge – that is now being overcome at leading international facilities.[30–33] Coulomb explosion imaging (CEI) is another emerging technique, that is increasingly finding use both as a route to exploring the fragmentation of multiply charged cations and as a means of probing molecules in the act of dissociating. Removing several electrons from an isolated molecule yields a multiply charged cation that dissociates by Coulomb explosion (CE). The term CE was introduced to describe and rationalise the fragment ions and their kinetic energy distributions following X-ray induced core ionisation of molecules like HI and CH_3I.[34] The earliest illustrations of CEI

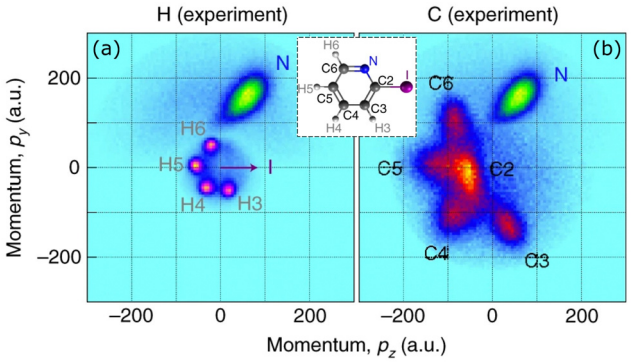

Fig. 2 Newton plots showing the absolute momenta of (a) N^+ and H^+ and (b) N^+ and C^+ fragment ions following CE of 2-iodopyridine (C_5NH_4I, structure shown in the inset). All data sets contributing to these plots involved detection of the I^+, N^+ and at least one H^+ and one C^+ ions, and the coordinate frame has been rotated so that in all cases the I^+ momentum points in the +z direction. (Adapted from Boll *et al.*, ref. 42, with permission from Springer Nature, copyright 2022.)

involved small molecular ions like CH_4^+, which were accelerated to high velocities and arranged to impact on, and pass through, a very thin (~3 nm thick) metal foil.[35,36] This interaction led to the stripping of further valence electrons, and CE. Determining the speeds and the directions of the resulting fragment ions allowed reconstruction of the parent cation structure at the instant of CE.

Short (femtosecond) duration laser pulses are now increasingly being used to initiate the CE of isolated molecules,[37–40] providing new insights into the structures of molecules and small clusters,[41–44] enabling the distinction of isomers[45,46] and even enantiomers[47,48] and the preparation of exotic cations.[49] Such experiments have, for example, recently allowed real-time studies of the Jahn–Teller driven distortions of the CH_4^+ cation.[50] Fig. 2 provides an impressive recent illustration, where CE methods have been used to reveal the momenta (and thus, after due processing, the positions) of all atoms within the 2-iodopyridine molecule. Note the constrained C^+ ion that was originally bonded to the I atom in the neutral parent molecule (C2 in Fig. 2). This Perspective has another focus: how CEI methods are offering new ways of exploring the fragmentation dynamics of multiply charged cations and, when used as the probe in pump–probe experiments, of neutral molecules and singly charged molecular cations.

Current laser-induced CEI studies partition into two broad families, distinguished by the way in which the CE is initiated. One uses the focussed fundamental output of, typically, a Ti-Sapphire laser providing near infrared (NIR) wavelengths around 800 nm to effect strong field ionisation (SFI).[51–54] The other employs one (or more) high-energy extreme UV (XUV) or soft X-ray photons, typically from a free-electron laser (XFEL).[55,56] In SFI, the neutral species of interest is elevated to (normally a range of) multiply charged states of the parent cation by the removal of several valence electrons. In soft X-ray excitation, in contrast, the wavelength is typically tuned to maximise the probability of removing one (or more) inner-shell electrons from a target nucleus (*i.e.* the initial excitation is much more site-specific) and the multiply charged states of the cation are formed by subsequent (rapid) Auger–Meitner (AM)[57] cascade. In both cases, the multiply charged cations then 'explode' by virtue of the Coulombic repulsion between the constituent nuclei. Determining the velocities and momenta of the charged products using contemporary time- and position-sensitive detectors allows a direct mapping of the positions of the charged nuclei in coordinate space, *i.e.* a non-spectroscopic view of the fragmentation dynamics.

Laser-induced CEI studies further sub-divide according to the specifics of the time and position-sensitive detection method. Much of the data reported in this article was obtained using multi-mass imaging methods, high count rates (>10 ions per laser shot) and covariance mapping techniques[58] to explore and establish possible correlations between different fragment ion pairs. An alternative approach, traditionally involving lower ion count rates and longer data accumulation times, relies on measuring coincidences between all fragment ions – as, for example, in the cold-target recoil-ion momentum spectroscopy (COLTRIMS) experiment used to generate the data shown in Fig. 2.

The illustrative examples that follow draw heavily on published and hitherto unpublished work performed in Bristol using NIR-SFI to induce CE but, when possible, the findings are compared and contrasted with those obtained when initiating CE by X-ray excitation (*i.e.* core ionisation). Note that some of the hitherto unpublished Bristol data are presented as ESI† to maintain a 'bigger-picture' narrative appropriate for a Perspective article.

II. Fragmentation of multiply charged molecular cations.

CF_3I and alkyl iodides

Fig. 3 shows time-of-flight (TOF) mass spectra of the fragment ions, after conversion to spectra of ion mass/charge (m/z) ratio, formed following 805 nm SFI of a jet-cooled CF_3I sample recorded at three different incident intensities: I = 260, 650 and 1300 TW cm^{-2}. We note that an ultrafast laser pulse presents a spatially and temporally varying spread of intensities and that there are many ways to report a laser intensity; the values reported here are peak intensities, calculated using *a priori* knowledge of the input beam conditions and profile.[59] The spectrum recorded at lowest I is dominated by peaks with m/z 127 (I^+) and 69 (CF_3^+), with weaker features at m/z 177 (CF_2I^+), 146 (IF^+), 139 (CI^+), 88.5 (CF_2I^{2+}), 63.5 (I^{2+}), 50 (CF_2^+) and 31 (CF^+). These same peaks appear in the spectra recorded at higher I, along with peaks at m/z 42 (I^{3+}), 34.5 (CF_3^{2+}), 25 (CF_2^{2+}), 19 (F^+), 15.5 (CF^{2+}), 12 (C^+), 9.5 (F^{2+}) and 6 (C^{2+}). The companion images show an obvious I^{4+} component within the m/z 31 signal measured at high I.[60] Knowing both the time and the position of arrival of each ion at the detector allows determination of the I-dependent velocity ($P(v)$) (and momentum $P(p)$) distributions of each fragment ion and identification of correlations between the various product ions, *i.e.* products arising *via* a common fragmentation process.

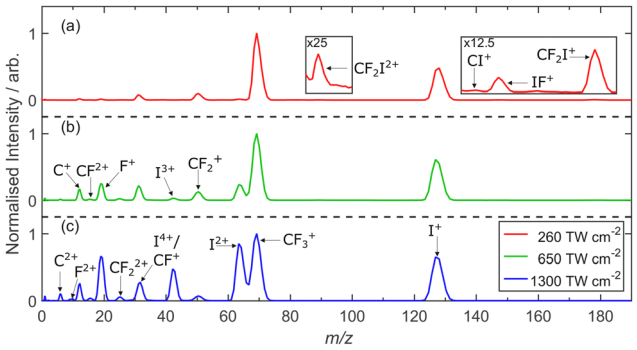

Fig. 3 TOF spectra of the fragment ions observed following 805 nm SFI of CF_3I at I = (a) 260, (b) 650 and (c) 1300 TW cm^{-2}, displayed with a mass/charge (m/z) scale, with the regions appropriate for CF_2I^{2+}, CI^+, IF^+ and CF_2I^+ ions shown on expanded vertical scales in the insets within panel (a). For ease of comparison, the spectra are displayed so that the m/z 69 (CF_3^+) peak appears with the same peak intensity in each.

These data, the results of analogous studies of the fragment ions from NIR SFI of CH_3I[59] and complementary *ab initio* trajectory simulations[61] all point to a continuum of behaviours for CF_3I^{Z+} parent ions, ranging from simple, 'diatomic-like' C–I bond fission at low Z, through a complex pattern of fragmentation behaviours involving loss of one or more F atoms (or ions) at intermediate Z, before approaching limiting Coulomb-driven dissociation at high Z ($> N$, where N is the number of atoms in the molecule), *i.e.* $Z > 5$ in these cases.

Here we focus on the low I data and the insights they provide into the fragmentation of CF_3I^{2+} cations. Fig. 4(a)–(d) show symmetrised images of the I^+ and CF_n^+ (n = 1–3) fragments, recorded with the laser polarisation vector, $\boldsymbol{\varepsilon}$, aligned vertically in the plane of the image, as shown in the top left-hand panel. All images displayed in this work are plotted using a linear false-colour scale that spans the maximum to minimum intensity recorded in the pixels within each image. Image analysis yields the respective velocity distributions, which are plotted as $P(p)$ distributions in Fig. 4(e). The low momentum features in the I^+ and CF_3^+ fragment distributions are attributable to rival dissociative ionisation (DI) pathways from singly charged CF_3I^+ parent ions and are not considered further.[60] The higher momentum features in these $P(p)$ distributions match well, consistent with 'diatomic-like' fragmentation of the CF_3I^{2+} dication, *i.e.*

$$CF_3I^{2+} \rightarrow CF_3^+ + I^+. \quad (1)$$

This channel had been identified previously in coincidence studies following XUV photoexcitation of CF_3I at discrete energies in the range 40–50 eV.[62] Covariance map images derived from the present data provide another way of identifying correlations between given pairs of fragments. Fig. 4(f) and (g) show, respectively, the (CF_3^+, I^+) and (CF_2^+, I^+) covariance images. In these depictions, the I^+ ion has been selected as the reference ion (and its velocity fixed to be vertically upwards – defined as $\phi = 0^\circ$ and illustrated by the red arrow in these panels) and the correlated 2-D velocity distribution of the CF_n^+ partner is then displayed in the frame defined by the reference ion. The correlations between the CF_3^+ and I^+ products are tightly focussed along $\phi = 180^\circ$, as required by momentum conservation in the case of a two-body dissociation. The correlation between the CF_2^+ and I^+ products is also centred along $\phi = 180^\circ$, but the covariance map image is more diffuse. This finding, and the evident similarities

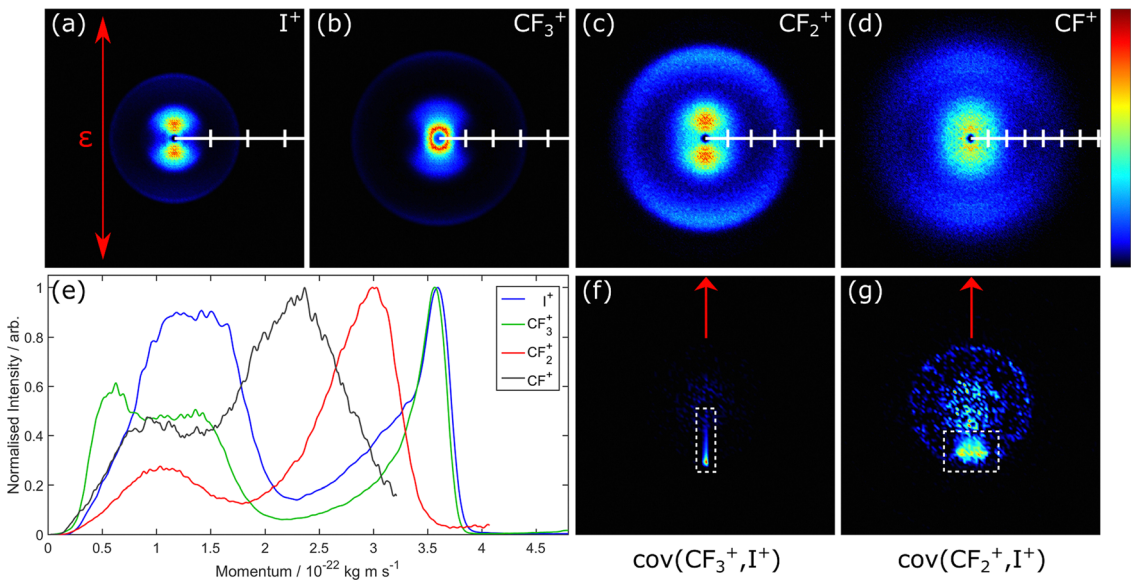

Fig. 4 Symmetrised images of the (a) I^+, (b) CF_3^+, (c) CF_2^+ and (d) CF^+ fragments formed by 805 nm SFI of CF_3I at I = 260 TW cm^{-2}. The ticks on the white horizontal scale on each image indicate 1000 m s^{-1} intervals. The $\boldsymbol{\varepsilon}$ vector of the SFI laser radiation is shown by the double headed red arrow in (a) and the relative signal intensities are shown using the linear false-colour scale that spans the maximum to minimum signal levels in the regions of interest within each image displayed at the end of the first row. The momentum distributions derived from these images are shown in (e). (f and g) Show, respectively, the (CF_3^+, I^+) and (CF_2^+, I^+) covariance map images, with the velocity of the I^+ reference ion chosen to be vertically upwards (shown by a red arrow) and the covariance signal of interest in each case bounded by dashed white lines.

between the various CF_n^+ velocity distributions, suggest that these CF_2^+ fragments arise by neutral F atom loss from internally excited primary CF_3^+ photoproducts. Covariance map image analysis also identifies a (more diffuse) correlation between I^+ and CF^+ products (consistent with loss of two F atoms or of F_2 from primary CF_3^+ products) and other charge symmetric fragmentation channels to $CF_2I^+ + F^+$ and to $CF_2^+ + IF^+$ product pairs, while the measured velocity distribution of the I^{2+} fragments also implies operation of the charge asymmetric $CF_3 + I^{2+}$ dissociation pathway.[60]

As noted above, some but not all the above fragmentation channels for CF_3I^{2+} cations had been identified in a previous study using photoelectron–photoion–photoion and TOF photoelectron–photoelectron–photoion–photoion coincidence spectroscopy methods.[62] Compared with CEI, such coincidence experiments, particularly when performed using tuneable XUV photons from a synchrotron, offer better control and definition of the excitation energy and the electronic state(s) in which the dication is prepared. But, as illustrated here, NIR SFI CEI measurements offer a substantial multiplex advantage (the present data sets reveal not just the various fragmentation channels for $Z = 2$ cations described here, but also provide information about the fragmentation of CF_3I^{Z+} ($Z > 2$) states, for which there is no prior experimental data, and can be undertaken in just a few hours using a table-top laser experiment.

Alkyl iodides, especially CH_3I, have featured in many imaging studies designed to explore CE dynamics. NIR SFI CEI studies of CH_3I[59,63–65] again illustrate the transition from 'diatomic-like' dissociation to $CH_3^+ + I^+$ products in the case of CH_3I^{2+} cations, where valence bonding forces compete with Coulomb repulsion,[63] through to Coulomb dominated dissociations yielding I^{q+} ($q \leq 6$) fragment ions at the highest intensities used in the Bristol experiments[59] and, as an extreme example, complete explosion to H^+, C^{p+} ($p \leq 4$) and I^{q+} ($q \leq 15$) fragments (*i.e.* from CH_3I^{Z+} cations with $Z \leq 22$) following absorption of multiple 5.5 keV X-ray photons.[66]

Many of the studies involving CH_3I where CE has been induced by one or more X-ray photons are ultrafast pump–probe studies, primarily designed to explore the ionisation and charge transfer (CT) dynamics as a function of time following an initial pump pulse that triggers C–I bond extension and progressive separation of the (neutral) I and CH_3 fragments. The results of an early experiment of this type, employing 1.5 keV probe photons, were interpreted in terms of (i) near-exclusive core ionisation of the iodine atom, (ii) subsequent fast (sub-femtosecond) AM decay leading to multiple positive charges localised on the iodine site and (iii) subsequent redistribution of this charge over the entire molecule, leading to fast Coulomb-repulsion dominated fragmentation.[67] At early pump–probe time delays (corresponding to small $H_3C\cdots I$ bond extensions), the time-dependent I^{q+} yields show clear evidence of CT from the I^{q+} to the CH_3 moiety (or, more accurately, electron transfer from the CH_3 to the multiply charged I^{q+} centre). We revisit such pump–probe data in Section III.

Here, we note that such a two-stage picture – AM decay leading to localised charging within part of the molecule and subsequent redistribution of this charge – is also often assumed in the case of XUV ionisation of molecules at their equilibrium geometry. Such processes probably merit further study. The valence electrons released after AM decay following core-ionisation at the equilibrium geometry emanate from molecular orbitals (MOs) that, in many cases, will be delocalised over the nuclear framework. Would the sequential picture outlined above for an alkyl iodide, in which the least tightly bound valence electrons in the ground state molecule are in 'atomic-like' p-orbitals localised on the I atom, extrapolate to, for example, XFEL induced ionisation of a non-polar molecule in which the least tightly bound electrons are in delocalised π orbitals?

Related questions apply when considering CE induced by NIR SFI, which lacks the initial site-specificity achieved by core-ionising a particular atom. Ionisation in this case is typically pictured as starting with the least tightly bound electrons; increasing the incident intensity leads to the progressive ejection of more of the less tightly bound valence electrons. NIR SFI might thus be expected to encourage simultaneous charging of multiple nuclei within a molecule. Again, however, alkyl iodides may not be 'general' test systems since, as noted above, the least tightly bound electrons in the ground state molecule are in orbitals localised on the I atom. So, even in the case of NIR SFI, the initial stages of the CE process in molecules like alkyl iodides, where the highest occupied MOs are localised non-bonding orbitals, may best be pictured as preferential charging of the I site and subsequent CT.

1,2-Dichloroethene

This example is chosen to illustrate the potential isomer selectivity afforded by CEI. Previous spectroscopic studies of the cations of both the *cis*- (or *Z*-) and *trans*- (or *E*-) isomers of 1,2-dichloroethene (DCE) have mainly focussed on the respective $Z = 1$ ions. Photoelectron spectroscopy methods have returned first adiabatic ionisation energies of both isomers ($IE \sim 9.65$ eV)[68,69] and insights into the low-lying excited electronic states of both cations.[70–72] Threshold photoelectron-photoion coincidence studies[73,74] have established the onset of the DI process

$$HClC{=}CHCl + h\nu \rightarrow H_2C_2Cl^+ + Cl + e^- \qquad (2)$$

at $E \sim 12.10$ eV for both isomers and *ab initio* calculations suggest rapid H atom migration following photoexcitation, so that the fragment ion in both cases is the C_{2v} symmetry $H_2C{=}CCl^+$ species.[74] The relative yields of $H_2C_2Cl^+$ fragment ions fall steeply at excitation energies $E > 16$ eV. $C_2H_2^+$ fragments dominate at these higher excitation energies and the shape of the energy-dependent breakdown curves suggests that these ions are formed by Cl loss from highly internally excited $H_2C_2Cl^+$ species. A (weaker) rival DI process yielding HC_2Cl^+ ions, by HCl elimination, has been observed at $E > 12.7$ eV and a further increase in the relative yield of HC_2Cl^+ fragment ions once $E > 17$ eV has been attributed to H atom loss from the primary $H_2C_2Cl^+$ species.[74,75] There are no documented DI channels for the $Z = 1$ parent cations yielding Cl^+ fragments.

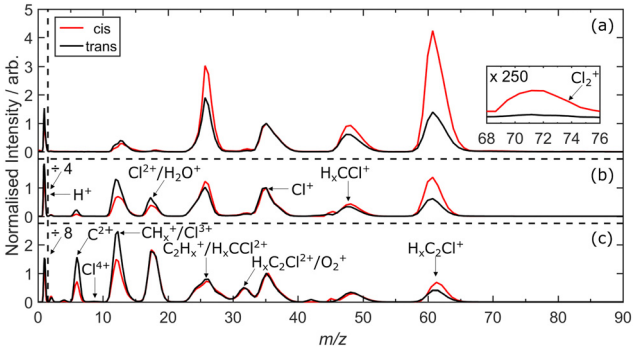

Fig. 5 TOF spectra of fragment ions observed following 805 nm SFI of *cis*- and *trans*-1,2-dichloroethene (red and black traces, respectively) at I = (a) 260, (b) 650 and (c) 1300 TW cm^{-2}, displayed with a mass/charge (m/z) scale. The various spectra have been plotted so that the Cl^+ peak is displayed with a common intensity and, for ease of display, the intensity of the H^+ peak (*i.e.* the m/z < 2 region) has been reduced by factors of 4 and 8 in panels (b and c), respectively. The inset in panel (a) highlights the relatively much greater yield of Cl_2^+ ions with v > 500 m s^{-1} from SFI of the *cis*-isomer at I = 260 TW cm^{-2}.

Fig. 5 shows m/z spectra of the fragment ions formed by 805 nm SFI of *cis*- and *trans*-1,2-DCE diluted in He (red and black traces, respectively) at I = 260, 650 and 1300 TW cm^{-2}, plotted so that the Cl^+ (m/z ~ 35.5) feature appears with a common peak intensity. Except at low m/z, the resolution of the present experiment is not sufficient to distinguish features differing by a single mass unit, but peaks attributable to $H_xC_2Cl^+$, H_xCCl^+, Cl^+, $C_2H_x^+$, CH_x^+ (x = 0–2) and H^+ ions are readily identifiable in the spectra recorded at I = 260 TW cm^{-2}, as are additional peaks assigned to Cl^{2+}, Cl^{3+} and C^{2+} ions when exciting at higher I. Contributions from the parent dication and from fragment cations like $HCCl^{2+}$, *etc.*, are not immediately assignable from the mass spectrum but are revealed by inspecting the m/z resolved images, as illustrated below.

Isomer dependent differences are immediately obvious in these m/z spectra, including a weak signal due to translationally excited Cl_2^+ products from *cis*-1,2-DCE (shown in the inset in Fig. 5(a)). The I-dependent images associated with these various fragment ions provide much new data about the fragmentation of higher Z states of 1,2-DCE. Here we focus particularly on the parent ions with Z = 2 and 3. Fig. 6 shows data for the H_xCCl^+ and H_xCCl^{2+} fragments (which, in both cases, are likely dominated by the x = 1 cations). To aid identification, all images and data pertaining to products from SFI of the *cis*-isomer are shown with a red frame. The images of the $HCCl^+$ (m/z ~ 48.5) ions from both isomers show an anisotropic ring of signal at large radius, the intensity of which peaks along the axis defined by ε. The images measured at low I also show an obvious central feature (attributable to parent dications), the relative intensity of which declines with increasing I. The $P(v)$ distributions of the $HCCl^+$ fragments from both isomers (Fig. 6(c)) are dominated by a peak at v ~ 2700 m s^{-1}. A higher velocity feature becomes increasingly evident at higher I. The $HCCl^{2+}$ image measured for both isomers at low I is weak, but the images recorded following NIR SFI at I = 1300 TW cm^{-2} show an obvious anisotropic ring of signal. The $P(v)$ distributions derived from these images peak at v ~ 3700 m s^{-1}, and both show clear tails extending to yet higher velocities. These data confirm the stability of the $HCCl^{2+}$ cation[76–78] and demonstrate the operation of two-body CE leading to C=C bond fission in both the Z = 2 and 3 parent ions, namely

$$HClC{=}CHCl^{2+} \rightarrow 2HCCl^+ \quad (3)$$

and

$$HClC{=}CHCl^{3+} \rightarrow HCCl^+ + HCCl^{2+}, \quad (4)$$

which are confirmed by the ($HCCl^+$, $HCCl^+$) and ($HCCl^+$, $HCCl^{2+}$) covariance image plots derived from the I = 260 TW cm^{-2} data shown in Fig. 6(d) and (e). (The more intense feature in the $\phi = 0°$ direction in the ($HCCl^+$, $HCCl^+$) covariance map image reflects autovariance, the correlation of a product ion with itself).

C–Cl bond fission occurs also, as evidenced by the (a) Cl^+ and (b) $H_xC_2Cl^+$ (our later analyses assume x = 2) fragment ion images shown in Fig. 7. The Cl^+ images from SFI of *trans*-1,2-DCE (Fig. 7(a)) show three features, each of which again maximise along the axis defined by ε. The $P(v)$ distribution derived from the image recorded at I = 260 TW cm^{-2} (Fig. 7(c)) peaks at v ~ 3500 m s^{-1} with obvious shoulders at both lower and higher v. The low v component fades in relative importance upon increasing I from 260 to 650 TW cm^{-2} but appears insensitive to further increases in I, whereas the highest v contribution becomes progressively more important as I increases. The Cl^+ images from SFI of *cis*-1,2-DCE return similar $P(v)$ distributions, though the low velocity component in the distribution formed at I = 260 TW cm^{-2} is relatively more important. Again, the low v component fades and the higher v component becomes relatively stronger with increasing I.

The $H_xC_2Cl^+$ fragment ion images from both isomers are similar (Fig. 7(b)) and show similar trends with increasing I. Each shows an intense central feature and an anisotropic ring at larger radius. The DI process (2) is likely to be the major contributor to the intense low velocity feature in the $H_xC_2Cl^+$ ion images. The relative magnitude of the higher velocity feature increases with increasing I. The mean momenta of these faster $H_xC_2Cl^+$ fragments match well with those of the most probable Cl^+ ions in the images recorded at low I, and this correlation is confirmed by the ($H_xC_2Cl^+$, Cl^+) covariance map images shown in Fig. 7(d) which, again, are tightly focussed along ϕ = 180°. As also deduced in recent XFEL enabled CE studies of these isomers following core-ionisation with 240 eV photons,[45,79] these fragments are attributable to a rival two-body dissociation of the Z = 2 parent cation, *i.e.*

$$HClC{=}CHCl^{2+} \rightarrow H_2C_2Cl^+ + Cl^+. \quad (5)$$

Similar analyses of the $H_xC_2Cl^{2+}$ fragment ion images recorded at higher I (Fig. S1 in the ESI†) imply the operation of an analogous C–Cl bond fission from the Z = 3 parent cations, *i.e.*

$$HClC{=}CHCl^{3+} \rightarrow H_2C_2Cl^{2+} + Cl^+. \quad (6)$$

The $P(v)$ distributions derived from the $H_xC_2Cl^{2+}$ ions are sensibly consistent with the faster component in the Cl^+ velocity distributions observed at higher I (Fig. 7).

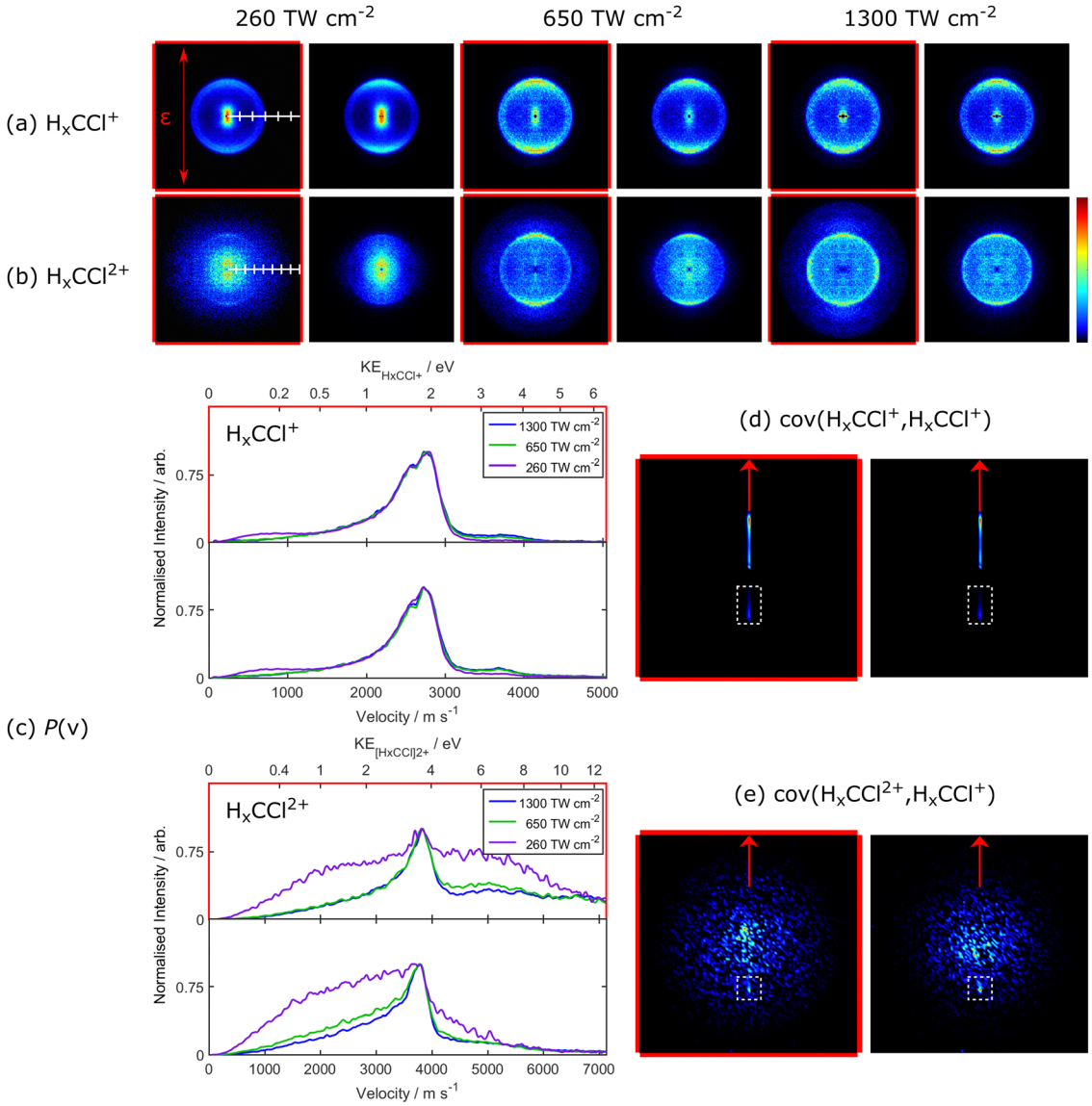

Fig. 6 Symmetrised images of the (a) H_xCCl^+ and (b) H_xCCl^{2+} fragments observed following 805 nm SFI of *cis*- (red borders) and *trans*-1,2-DCE at I = 260, 650 and 1300 TW cm^{-2}. The laser polarisation vector, $\boldsymbol{\varepsilon}$, is vertical in the plane of the image, as shown in the top left-hand panel and the relative signal intensities are shown by the linear false-colour scale chosen to span the maximum to minimum signal levels in the regions of interest within each image at the end of row (b). The ticks on the white horizontal scale in the left-hand image in each row indicate 1000 m s^{-1} intervals. The $P(v)$ distributions of the H_xCCl^+ and H_xCCl^{2+} fragments from each parent isomer are shown in (c) with, in each case, the maximum signal scaled to an intensity of unity. The corresponding fragment kinetic energies are shown on the top x axis. (d and e) Show, respectively, the (H_xCCl^+, H_xCCl^+) and (H_xCCl^{2+}, H_xCCl^+) covariance map images from analysis of I = 260 TW cm^{-2} data from the *cis*- (left) and *trans*-isomers (right), selecting H_xCCl^+ as the reference ion and fixing its velocity to be vertically upwards, as indicated by the red arrow. The covariance signal of interest in each case is bounded by dashed white lines, while the more intense feature along the ϕ = 0° axis in both images in (d) is the autovariance signal.

This section devoted to 1,2-DCE ends with data for the $C_2H_x^+$ fragment ions (Fig. 8), which are henceforth assumed to be $C_2H_2^+$. The images of these products from both parent isomers show an intense central feature, and an isotropic signal stretching to larger radius which becomes relatively more important at higher I. The central feature is attributable to $C_2H_2^+$ products from secondary decay (Cl atom loss) of internally excited $H_2C_2Cl^+$ products arising *via* DI channel (2).[74,75] The $P(v)$ distributions derived from the $C_2H_2^+$ images are shown in Fig. 8(b). The distributions obtained at lowest I both peak at $v \sim 1400$ m s^{-1}. Excitation at this (relatively) low intensity will strongly favour formation of parent ions with low Z and the major source of these $C_2H_2^+$ ions is, again, secondary decay of the internally excited primary $H_2C_2Cl^+$ fragments formed, in this case, by the CE process (5).

Both $P(v)$ distributions also show a 'tail' stretching to higher v, that gains in relative importance at higher I. The form of this 'tail' is isomer-specific, stretching to considerably higher v in the case of the *cis*-isomer. The ($C_2H_2^+$, Cl^+) covariance plots derived from the I = 260 TW cm^{-2} data for both isomers show

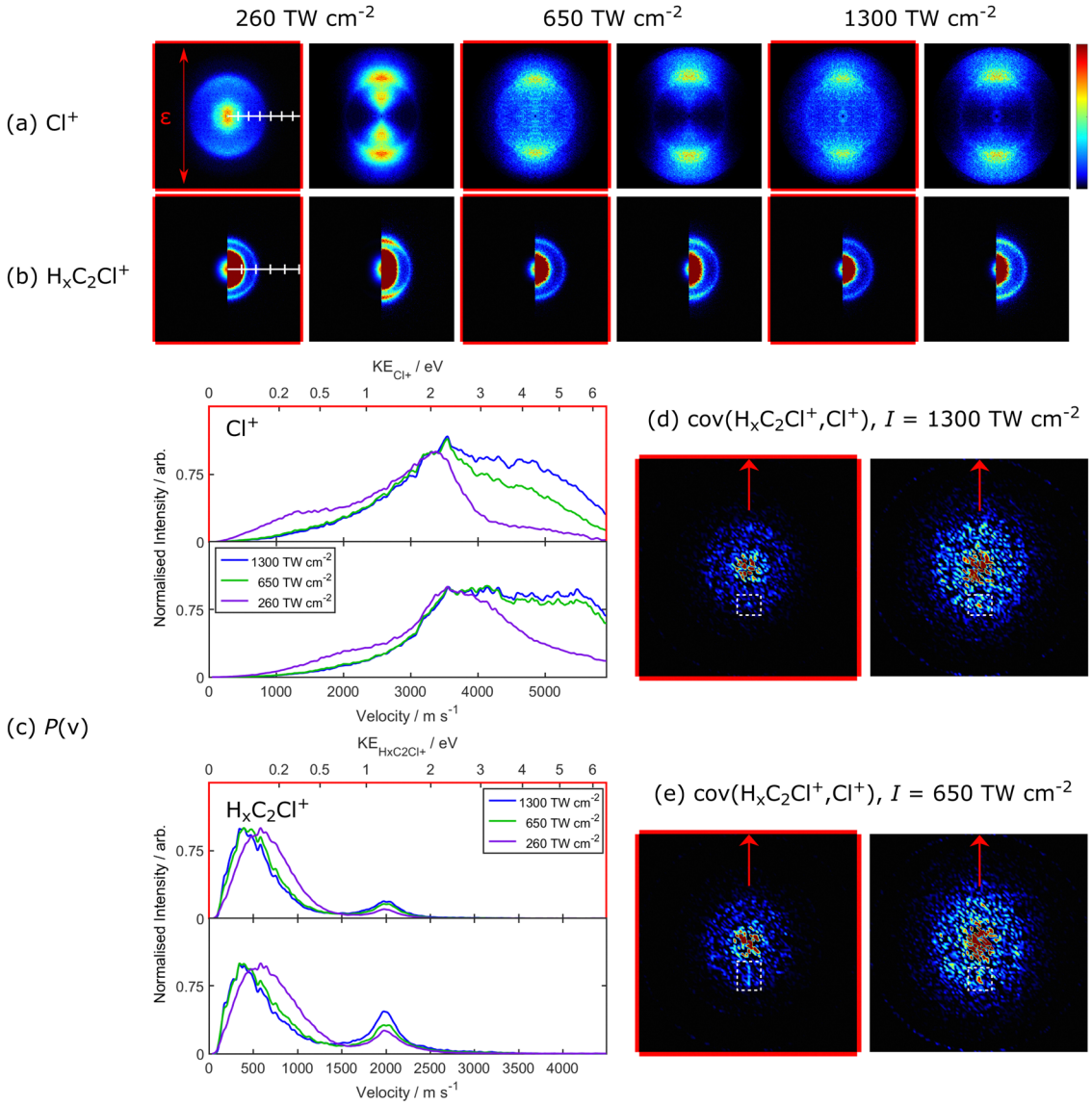

Fig. 7 Symmetrised images of the (a) Cl^+ and (b) $H_xC_2Cl^+$ fragments observed following 805 nm SFI of *cis*- (red borders) and *trans*-1,2-DCE at I = 260, 650 and 1300 TW cm^{-2}. ε is vertical in the plane of the image, as shown in the top left-hand panel, and the ticks on the white horizontal scale in the left-hand image in rows (a and b) indicate 1000 m s^{-1} intervals. The relative signal intensities in the images in row (b) are displayed using the same linear false-colour scale as in row (a) and on a 100× increased scale (left and right half images, respectively). (c) $P(v)$ distributions of the Cl^+ and $H_xC_2Cl^+$ fragments from each parent isomer with, in each case, the maximum signal scaled to an intensity of unity. These confirm that the Cl^+ images recorded at higher I extend to (and beyond) the edge of the detector area. (d) and (e) ($H_xC_2Cl^+$, Cl^+) covariance map images obtained following SFI of each isomer at I = 1300 and 650 TW cm^{-2}, respectively. In all cases, Cl^+ has been selected as the reference ion (and its velocity fixed to be vertically upwards, indicated by the red arrow) and the (weak) covariance signals of interest are bounded by dashed white lines.

obvious, but diffuse, correlations (Fig. 8(c)). These results all point to three-body CE from the Z = 3 parent ions

$$HClC{=}CHCl^{3+} \rightarrow HCCH^+ + Cl^+ + Cl^+, \qquad (7)$$

a view supported by photoion–photoion–photoion coincidence (PIPIPICO) measurements of these same three fragments arising *via* CE of both 1,2-DCE isomers induced by either 240 eV core-ionisation[45] or ultrafast NIR SFI.[80] Fig. 9 depicts the derived fragment ion correlations from a NIR SFI study in so-called Newton plots, in which the momenta of two fragment ions (here $C_2H_2^+$ and Cl^+) are plotted with respect to the momentum of the third fragment (Cl^+). The Newton plot for *trans*-1,2-DCE (Fig. 9(b)) shows the two Cl^+ fragments recoiling in essentially opposite directions, with the $C_2H_2^+$ fragment remaining almost at rest, as would be predicted in the case of a near-instantaneous explosion from the undistorted equilibrium geometry where the centre of mass of the C_2H_2 moiety is symmetrically positioned between the two Cl atoms. The corresponding plot for *cis*-1,2-DCE (Fig. 9(a)) is obviously different: the angle between the two Cl^+ fragment momenta is ~108° and the $C_2H_2^+$ product has significant momentum. Both Newton plots imply that the CE giving rise to these fragments

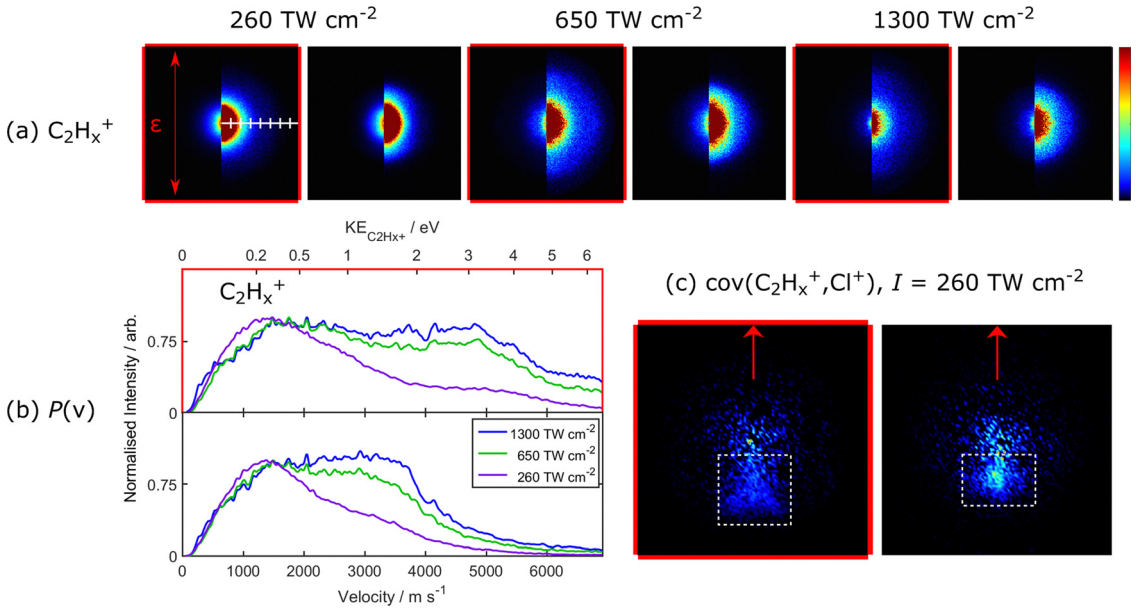

Fig. 8 (a) Symmetrised images of the $C_2H_x^+$ fragments observed following 805 nm SFI of *cis*- (red borders) and *trans*-1,2-DCE at I = 260, 650 and 1300 TW cm^{-2}. The data are plotted using the linear false-colour scale shown at the far right of this row (left halves) and on a 10× expanded scale (right halves), wherein more of the central feature (attributed to $C_2H_2^+$ ions from secondary decay of $H_2C_2Cl^+$ products formed in the DI channel (2)) has deliberately been saturated to reveal the faster component of these $P(v)$ distributions more clearly. $\boldsymbol{\varepsilon}$ is vertical in the plane of the image, as shown in the top left-hand panel. (b) $P(v)$ distributions of the $C_2H_x^+$ fragment ions derived from these images. (c) Covariance map images from analysis of I = 260 TW cm^{-2} data for *cis*- (left) and *trans*-1,2-DCE (right), selecting Cl^+ as the reference ion (and fixing its velocity to be vertically upwards, indicated by the red arrow) and displaying the correlated 2-D velocity distributions of the $C_2H_x^+$ fragments in the frame defined by the reference ion. The covariance signal of interest in each case (bounded by dashed white lines) is relatively 'fuzzy', but notably more extensive in the case of the *cis*-isomer.

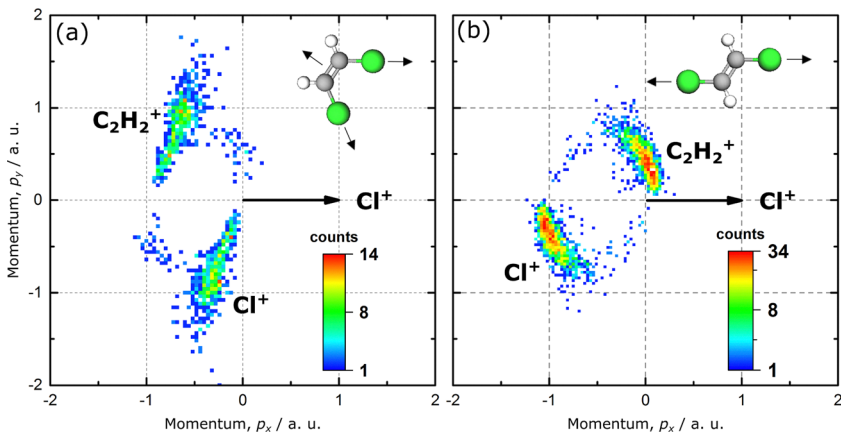

Fig. 9 Newton plots of the products arising from the triple coincidence channel (process (7)) following NIR SFI of (a) *cis*- and (b) *trans*-1,2-DCE. The momenta of the $C_2H_2^+$ fragment (upper half) and one of the Cl^+ fragments (lower half) are displayed in the frame of the momentum of the second Cl^+ fragment, which is shown as a horizontal black arrow. The momentum vectors of the $C_2H_2^+$ fragment and the first Cl^+ fragment are normalised to the length of the momentum vector of the second Cl^+ fragment (reproduced from ref. 80, with permission).

occurs in a (close to) simultaneous manner. Similar behaviour was identified in XUV (140 eV) photoinduced CE studies of the *cis*- and *trans*-isomers of 1,2-dibromoethene.[79] Total energy conservation requires that the Cl^+ fragments formed *via* CE process (6) of *trans*-1,2-DCE should have greater average kinetic energy than those from the *cis*-isomer, and that the CE of *trans*-1,2-DCE should yield the more translationally excited $C_2H_2^+$ products. Such expectations are borne out by comparing the high v ends of the respective $P(v)$ distributions of the Cl^+ fragments obtained at higher I (Fig. 7(c)) and by the more extensive ($H_2C_2^+$, Cl^+) covariance map following SFI of *cis*-1,2-DCE (Fig. 8(c)).

The m/z spectra following NIR SFI of the two isomers illustrate another isomer specific difference relating to the weak peak at $m/z \sim 71$, due to Cl_2^+ ions, that is not apparent when plotted with the intensity scale used in Fig. 5. The associated images are dominated by a central (*i.e.* zero kinetic

energy) feature, attributable to ionisation of trace Cl_2 impurity in the respective samples. But the $P(v)$ distribution of the Cl_2^+ fragments from SFI of *cis*-1,2-DCE at I = 260 TW cm^{-2} also shows some translationally excited fragments (peaking at $v \sim 1000$ m s^{-1}) which are not present in the corresponding distributions from the *trans*-isomer. This difference is highlighted in the inset in Fig. 5(a), which only shows a measurable yield of Cl_2^+ fragments with $v > 500$ m s^{-1} from SFI of *cis*-1,2-DCE. (Cl_2^+, $C_2H_2^+$) and ($C_2H_2^+$, Cl_2^+) covariance map images (Fig. S2 in the ESI†) from analysis of the images taken at I = 260 TW cm^{-2} confirm that these Cl_2^+ fragments arise *via*

$$cis\text{-HClC=CHCl}^{2+} \rightarrow Cl_2^+ + HCCH^+, \quad (8)$$

which likely involves a four-centre transition state involving Cl–Cl bond formation in tandem with C–Cl bond rupture.

Summarising, new fragmentation behaviour provided by CEI studies of *cis*- and *trans*-1,2-dichloroethene include the operation of rival charge symmetric C=C and C–Cl bond fission channels from the dication of both isomers, as well as Cl_2^+ elimination from *cis*-1,2-DCE (processes (3), (6) and (8)). CEI also reveals that Z = 3 parent ions decay by C=C bond fission and by two triple dissociation processes. One, a near-concerted process (7), releases two Cl^+ fragments with clearly isomer specific kinematics. The other is attributable to secondary decay of internally excited $H_2C_2Cl^{2+}$ fragments formed *via* process (6).

This represents just one of a rapidly growing number of triple dissociations investigated using ultrafast laser induced CEI, often in conjunction with so-called native-frame analysis wherein successive steps in a sequential three-body fragmentation are analysed in their own 'native' frame of reference.[81] Such methods have recently been used to demonstrate that, for example, the three-body dissociation of the OCS^{3+} cation proceeds sequentially, *via* rival channels yielding CO^{2+} and CS^{2+} intermediates that decay further over a longer time scale.[81] As in the case of 1,2-DCE, the triple dissociation of $C_2H_4Br_2^{3+}$ cations to $C_2H_4^+ + 2Br^+$ products is best viewed as involving both concerted and non-concerted contributions,[82] as are the dissociations of the trications of both 1- and 2-iodopropane to $CH_3^+ + C_2H_4^+ + I^+$ products (*via* a $C_3H_7^{2+}$ intermediate in the asynchronous dissociations)[83] and of $CHBr_3^{3+}$ cations to $CHBr^+ + 2Br^+$ (with a $CHBr_2^{2+}$ intermediate in the non-concerted pathway).[84]

Summary

Table 1 illustrates many of the polyatomic molecules for which one or more of their polycation fragmentations have now been investigated by CEI methods. A critic could argue that many of these studies reveal active fragmentation channels rather than the fragmentation dynamics *per se*. It is striking that the $P(v)$ (and the kinetic energy) distributions of the fragments arising *via* many of the charge symmetric binary dissociations are relatively narrow – see channels (1) (Fig. 4) and (3) (Fig. 6) and (5) (Fig. 7) in this work – notwithstanding the apparent energetic imprecision of the NIR SFI or XUV core-ionisation process that led to their formation. But the appearance of, for example, CF_2^+ (or $C_2H_2^+$) fragments attributable to secondary decay of CF_3^+ ($H_2C_2Cl^+$) products in the examples reviewed here also implies that some of these primary fragments are formed with sufficient internal energy to enable subsequent unimolecular decay. More coincidence studies that provide energetic information about not just the fragment ions but also the photoelectrons formed upon multiple ionisation would surely be revealing. The growing number of studies of the three-body dissociation of parent trications are providing more dynamical insights, and the application of covariance and native frames analysis methods are allowing discrimination between concerted (or at least near concerted) and sequential fragmentations. However, a common finding is that a given trication displays a mix of both behaviours and there is still a way to go before one could determine, for example, whether these different outcomes reflect rival fragmentation dynamics from a common electronic state or dissociation from two (or more) different states of the photo-prepared trications. Three-body fragmentations where one fragment is released as a neutral species also remain a challenge but, again, the recent literature includes evidence of much progress.[85–88]

Table 1 Triatomic and larger molecules for which the fragmentation of their polycations (with charge Z+) have been investigated by ultrafast laser induced CEI methods. Molecules are listed in order of increasing size. The numbers in parentheses indicate the range of Z values investigated in the various cited works. Ionisation in these studies was induced by NIR SFI, apart from in those references shown in bold font which employed XUV or X-ray core excitation

Species (Z states); ref.	
H_2O and D_2O (2,3);[89–93,**94**]	H_2S (3);[95]
CO_2 (2–9);[90,96–107]	OCS (2–4);[90,108–112]
CS_2 (3–10);[113–118]	O_3 (3);[119]
SO_2 (2,3);[120]	N_2O (3–8);[121,122]
NO_2 (2–6);[99,123]	
C_2H_2 (2–4);[124–131]	H_2CO (2–4);[132,133]
CH_4 (2);[134]	CH_3Cl (2,3);[135]
CH_3I (many);[59,63,136,137,**138**]	$CHBr_3$ (2–5);[84,139]
CHBrClF (4–5);[47]	CF_3I (2–5);[60]
HCOOH (2);[140,141]	
C_2H_4 (2);[142]	CH_3OH (2,3);[143–151,**152**]
CH_3SeH (many);[153]	CH_3CN (2);[154–156]
$C_2H_2Cl_2$ (3);[45]	1,2-$C_2H_2Br_2$ (2,3);[79]
ClC(O)SCl (2,3);[157]	
C_3H_4 (allene) (2,3);[158–160]	C_3H_4 (methyl acetylene) (2,3);[161,162]
CH_3NH_2 (2);[163]	
1,2-$C_2H_4Br_2$ (2,3);[164,165]	1,2-C_2H_4BrCl (2);[166,167]
1,2-$C_2H_4Cl_2$ (2);[168]	1,2-C_2H_4FBr (2);[169]
C_2H_5OH (2);[150,170,**171**]	$CH_3OC(O)SCl$ (2,3);[172]
CH_3COCH_3 (2);[150]	$(CH_2OH)_2$ (2);[150]
1,2-C_3H_7I (2,3);[83]	C_3H_7OH (1-/2-propanol) (2);[**87**,150]
C_4H_8 (1,3-butadiene) (3);[173,174]	$C_4N_2O_2H_3I$ (5-iodouracil) (many);[**175**]
C_6H_6 (3);[176]	$C_6H_3F_2I$ (2,6-/3,5-difluoroiodobenzene) (3);[**177**]
$(CH_3)_3COH$ (2);[150]	C_6H_{12} (cyclohexane) (2);[178,179]

Table 2 Fragmentation studies involving isolated polyatomic molecules and singly- and doubly-charged molecular cations explored by ultrafast pump–probe experiments using CEI probe methods

Molecule	Pump + probe method[a] ref.
H_2CO	UV + NIR[180,181]
CH_3I	NIR + NIR;[182] NIR + X;[67,183] UV + NIR;[184–187] UV + X[188]
CH_2ClI	UV + NIR[185]
CH_2BrI	UV + X[189,190]
$(CH_3)_2CHI$	UV + X[191]
$C_6H_3F_2I$	UV + X[188]
$C_2H_5CH(CH_3)CH_2I$	UV + X[192]
OCS^+	NIR + NIR[193]
SO_2^+	NIR or UV + NIR[194]
CH_3I^+	X + NIR[195]
$C_2H_5OH^+$	NIR + NIR[196]
1,2-$C_3H_7OH^+$	NIR + NIR[197]
$C_2H_2^{n+}$ (n = 1–3)	X + X[198,199]
$C_2H_5OH^{2+}$	X + X[200]

[a] UV = ultraviolet pump wavelength, X = XUV or X-ray, NIR = near infrared.

III. Using CEI probe methods to track the photofragmentation of neutral molecules

Alkyl iodides

CEI methods are increasingly also finding use in two-colour studies of the fragmentation dynamics of photoexcited neutral molecules, and singly charged cations. Table 2 lists illustrative studies involving polyatomic (larger than diatomic) species. Again, the alkyl iodides are proving to be popular test systems.

(i) NIR-SFI probing. Fig. 10 compares images of the CF_3^+, I^+ and I^{2+} ions formed in a two-colour experiment performed in Bristol involving a jet-cooled sample of CF_3I in He, 267 nm pump photons and 805 nm SFI ($I \sim 1300$ TW cm^{-2}) at eight different pump probe time delays in the range -390 fs $\leq \delta t \leq 1$ ns. In each case, the raw two-colour image (and the corresponding NIR-only image) has been centred, symmetrised and 'cleaned' by re-setting any extreme signals associated with hot pixels. The difference images shown in Fig. 10 were then derived by subtracting the NIR-only signal from the two-colour image to minimise the one-colour contribution at each δt and, simply for the present illustration purposes, the intensity in any pixels returning a negative difference signal were then reset to zero. Each image is displayed in two halves, with the right half plotted on a 10× expanded intensity scale to reveal weaker features induced by the 267 nm pump pulse more clearly. The original (symmetrised) images, without the NIR-only background subtraction, are shown in Fig. S3 in the ESI.†

All I^+ images obtained at $\delta t > 0$ show a ring displaying parallel recoil anisotropy (*i.e.* with v aligned preferentially parallel to ε), labelled DISS (for 'dissociation'). A much weaker DISS feature is discernible in the corresponding CF_3^+ images. As shown below, the associated velocities confirm that these DISS features are signatures of the well-characterised 267 nm photolysis of CF_3I, yielding neutral CF_3 and I fragments, one or other of which is subsequent ionised (by NIR SFI) to a CF_3^+ or I^+ ion.

These are the only features in these images that report directly on the field-free fragmentation of CF_3I (*i.e.* are unperturbed by the probe NIR SFI process), but the CF_3^+, I^+ and I^{2+} images recorded in the range $0 \leq \delta t \leq 600$ fs each show additional features (two in the case of the CF_3^+ images) labelled

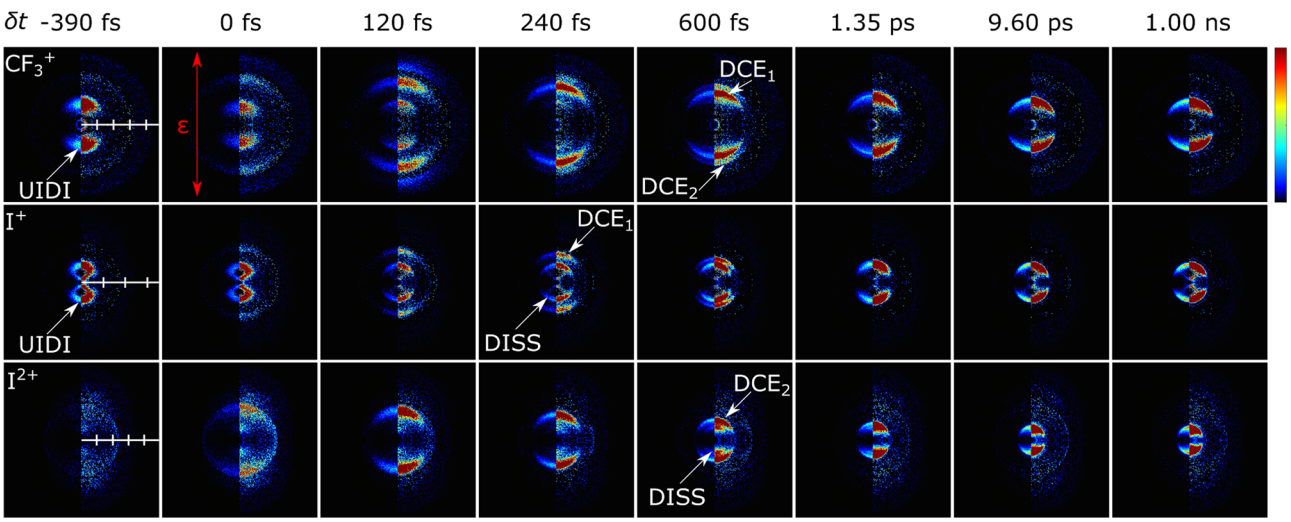

Fig. 10 Symmetrised images of the CF_3^+, I^+ and I^{2+} fragments from ultrafast two-colour (267 nm pump–805 nm SFI probe, $I = 1300$ TW cm^{-2}) studies of CF_3I at different time delays in the range -390 fs $\leq \delta t \leq 1$ ns after subtracting the one-colour contribution obtained with just the NIR pulses. The ε vector of both laser beams is vertical, in the plane of the detector, as indicated by the double-headed arrow in the $\delta t = 0$ CF_3^+ image and illustrative examples of the various channels are labelled with the acronyms defined in the text. The relative intensities in images displayed in any one row are depicted using a common linear false-colour scale spanning the maximum through minimum signal values shown at the far right (left halves) and on a 10× expanded scale (right halves).

DCE_1 and DCE_2 (for 'dynamic Coulomb explosion'), with radii that decrease with increasing δt. These features are better viewed *via* the false-colour 2-D maps showing the integrated (over all angles) ion yields as functions of velocity and δt (over the range $-0.45 \leq \delta t \leq +10$ ps) shown in Fig. 11. The maps displayed here are derived from images such as those shown in Fig. 10, *i.e.* after subtracting the optimum amount of the corresponding one-colour (NIR-only) image and resetting any resulting negative intensities to zero. The corresponding maps without the one-colour subtraction are shown in Fig. S4 in the ESI.† As Fig. 11(a) shows, this procedure leaves some residual noise at velocities associated with the one-colour NIR-only SFI signal (labelled ISFI) but clearly accentuates the two-colour features of current interest. Analogous CF_3^+, I^+ and I^{2+} maps obtained using a lower NIR intensity ($I \sim 650$ TW cm^{-2}) are displayed in Fig. S5 in the ESI.†

The features labelled DCE_1 and DCE_2 in Fig. 11 and Fig. S5 (ESI†) arise from SFI of the CF_3 and I co-fragments from photodissociation of a common parent molecule. Post-SFI, the resulting $CF_3^+ + I^+$ and $CF_3^+ + I^{2+}$ ion pairs then Coulomb repel each other with a force that scales inversely with their separation, yielding the respective DCE_1 and DCE_2 signals. The velocities of these fragment ions are thus δt-dependent, as illustrated schematically in Fig. 12 (along with the mechanism responsible for the accompanying one-color ISFI signal). The CF_3^+ products attributable to DCE_1 and DCE_2 merge at long δt with those arising *via* the DISS process, as shown in Fig. 11(a) and Fig. S5(a). Equivalent plots for the I^+ and I^{2+} yields recorded in the same two-colour multi-mass imaging experiments are shown in Fig. 11(b) and (c). The I^+ plot shows the DISS feature much more clearly and confirms the carrier of the DCE_1 feature. As Fig. 11(d) shows, the momentum ($P(p)$) distributions of the CF_3^+, I^+ and I^{2+} fragments sampled at long time delay ($\delta t \sim 1$ ns) all match well, support previous conclusions that most (>90%) of the iodine atoms formed following excitation of CF_3I molecules at 267 nm are in the spin–orbit excited ($^2P_{1/2}$) rather than ground ($^2P_{3/2}$) state (henceforth identified as I* and I, respectively)[201–203] and imply similar NIR SFI probabilities for both spin–orbit states of the I atom.

Several further aspects of these data merit note. First, the DISS feature is relatively much stronger in the I^+ than the CF_3^+ map, implying that the probability of NIR strong field induced one photon ionisation of I is much greater than that of CF_3 under the prevailing experimental conditions. A weak DISS feature is even observable in the I^{2+} map (particularly that recorded at lower I, Fig. S5(c), ESI†). Second, as can be seen from comparing the corresponding maps in Fig. 11 and Fig. S5 (ESI†), the relative intensities of signals arising *via* the DISS and DCE channels are I-dependent. Such is to be expected, since the relative probability of ionising both partners (*i.e.* of generating DCE signals) increases with I. Third, the signal to noise (S/N) ratios in the data measured at $I \sim 1300$ TW cm^{-2} are sufficient

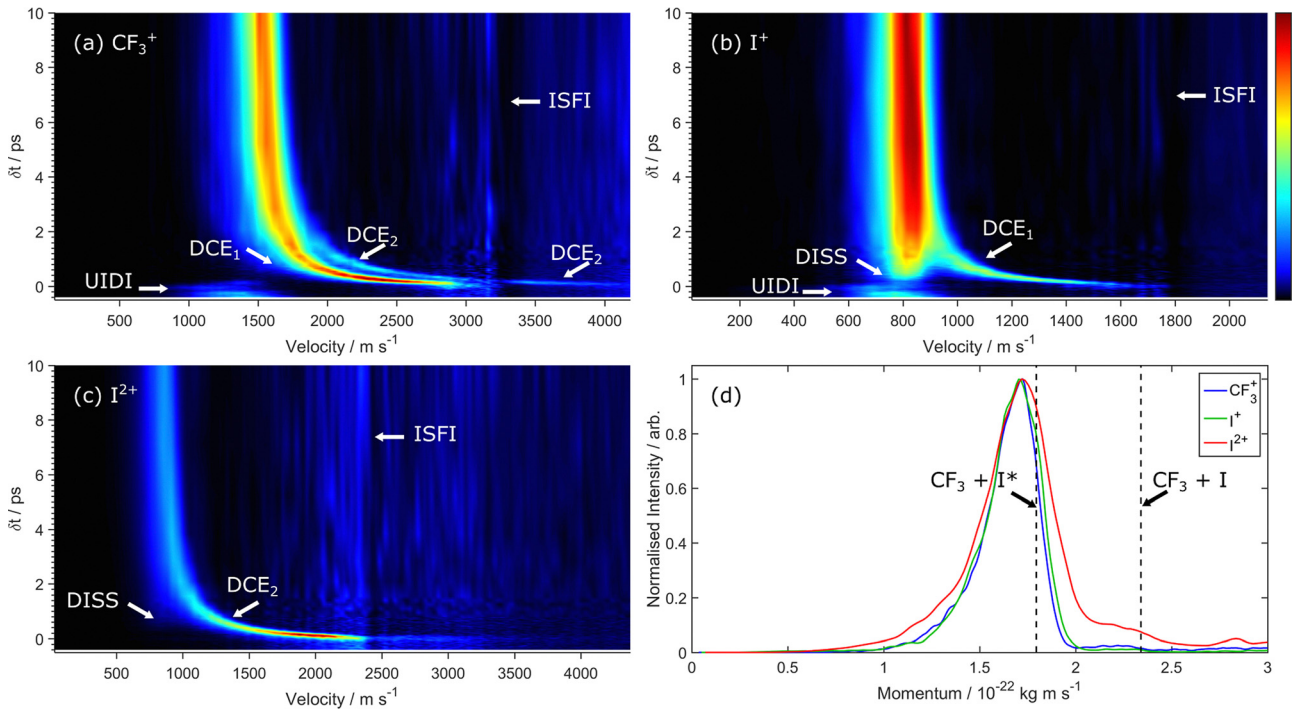

Fig. 11 2-D false-colour maps showing (a) CF_3^+, (b) I^+ and (c) I^{2+} ion velocities following 267 nm photolysis of CF_3I as a function of δt obtained by angular integration of images like those shown in Fig. 10, recorded with 805 nm intensities $I \sim 1300$ TW cm^{-2}, with the various channels labelled using the acronyms introduced in the text. The relative intensities in each panel are depicted using the linear false-colour scale shown to the right of panel (b). (d) $P(p)$ distributions of the CF_3^+, I^+ and I^{2+} ions obtained by integrating data measured over the delay range $0.1 \leq \delta t \leq 1$ ns, with the maximum p values associated with primary photodissociation of $CF_3I(v = 0)$ molecules to form $CF_3(v = 0)$ radicals together with ground (I) and spin–orbit excited (I*) atoms indicated. Each distribution has been scaled so that the features associated with CF_3 + I* products have the same peak intensity.

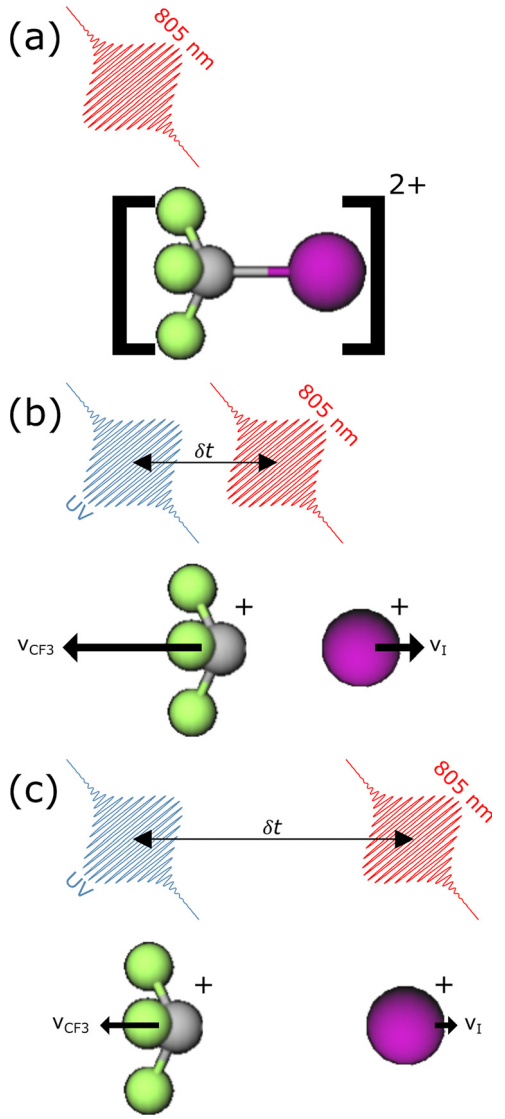

Fig. 12 Illustration of the sources of important signatures evident in UV pump −805 nm SFI probe experiments at different time delays, δt, using CF_3I as the exemplar and assuming removal of two electrons and a symmetric charge separation. (a) CF_3I^{2+} formation by 805 nm SFI alone, or with the UV and 805 nm pulses coincident in time (*i.e.* δt = 0). The subsequent CE of these dications results in the CF_3^+ and I^+ products identified with the label ISFI in the respective 2-D maps. (b and c) CF_3^+ and I^+ fragments formed by 805 nm SFI (at progressively later delays δt) of neutral CF_3 and I products formed by UV excitation at t = 0. The neutral photoproducts are formed with characteristic, thermochemically determined, recoil velocities (equal to that of the feature(s) labelled DISS in the 2-D maps). Subsequent SFI of these neutral fragments introduces an additional Coulombic repulsive contribution to the measured CF_3^+ and I^+ velocities, the magnitude of which decreases with increasing δt (*i.e.* increasing inter-ion separation) as illustrated by the velocity vectors in (b and c). This process is responsible for the characteristic DCE signals, the velocities of which converge to that of the DISS component at long δt.

to reveal DCE following NIR SFI of geminate CF_3 and I fragments to $CF_3^+ + I^{3+}$ pairs (process DCE_3, illustrated in Fig. S6(a) in the ESI†). Finally, the CF_3^+ and I^+ maps both show a diffuse low velocity feature at $\delta t < 0$ labelled UIDI in Fig. 11 and Fig. S5 (ESI†). This feature is attributable to UV induced photodissociation of CF_3I^+ ions formed by NIR SFI yielding, respectively, $CF_3^+ + I$ and $CF_3 + I^+$ fragments with kinetic energies consistent with those reported in previous VMI studies of the UV photodissociation of CF_3I^+ cations.[204]

Fig. 13 shows analogous false-colour 2-D maps of the integrated CH_3^+, I^+ and I^{2+} ion yields from the corresponding ion images (after subtracting the one-colour NIR SFI contribution, shown in Fig. S7 in the ESI†) as functions of velocity and δt, following 267 nm photolysis of CH_3I and 805 nm SFI with I = 1300 TW cm^{-2}. Fig. 13(d) shows the respective $P(p)$ distributions sampled at long time delay ($\delta t \sim 1$ ns) which, again, confirm previous findings of the ∼70 : 30 I* : I product ratio following CH_3I photolysis at this wavelength and the formation of some $CH_3(v_1 = 1)$ + I products (revealed by the bump on the low momentum side of the relevant peak in the $P(p)$ distribution).[205,206] Again, the 'raw' data obtained prior to subtracting the one-colour NIR SFI contributions are shown in the ESI† (Fig. S8 in the ESI†). Similar 2-D plots recorded at lower NIR SFI probe intensities ($I \sim 650$ TW cm^{-2}) are displayed in Fig. 14 (below) and in Fig. S9 in the ESI† (before and after subtracting the NIR SFI contribution, respectively). These CH_3I data show obvious similarities with those reported previously in the seminal studies of Corrales *et al.* using significantly lower NIR intensities[184,186] but, again, some of the relative intensities are clearly I dependent. The CH_3^+ and I^+ maps both show DISS features attributable to UV photodissociation of CH_3I to CH_3 products together with I/I* products followed by single ionisation of one or other product by NIR SFI. The DISS feature is weak (at best) in the I^{2+} map, reflecting the improbability of doubly ionising an I/I* fragment without also at least singly ionising its CH_3 radical partner. All three maps also show features labelled DCE_1 and/or DCE_2, converging to the asymptotic velocities of the CH_3 + I* and CH_3 + I products at long δt.[59,185,186] Again, the S/N ratios in the present data are sufficient to reveal a DCE_3 feature in the 2-D map derived from the I^{3+} images (see Fig. S6(b), ESI†).

The DCE_1 feature(s) can be revealed yet more clearly by coincidence imaging measurements. Fig. 14 compares such coincidence imaging data for the CH_3^+ and I^+ products formed following 267 nm photolysis of CH_3I and subsequent NIR SFI probing (laser pulse duration ∼23 fs, $I \sim 280$ TW cm^{-2}) recorded at delays $\delta t \leq 4$ ps with the corresponding data ((c) and (d)) from multi-mass imaging data studies using NIR SFI probing at $I \sim 650$ TW cm^{-2}. Removing all non-coincident sources of these singly charged fragment ions reveals four clear features in the overall $P(v)$ distributions: two time-invariant components arising from ISFI, yielding CH_3^+ ions together with $I^+(^3P_2)$ and (unresolved) $I^+(^3P_{1,0})$ products from CE of CH_3I^{2+} parent ions, and two time-dependent features from NIR SFI of geminate pairs of separating CH_3 and I (I*) fragments resulting from UV photoexcitation (DCE_1).[187]

As with CF_3I, non-coincident maps derived from multi-mass imaging experiments can show additional features attributable to processes other than the field-free fragmentation of CH_3I that is of primary interest in the current context. The CH_3^+ and I^+ maps recorded at lower I (*e.g.* Fig. S9 and, particularly, S10 in

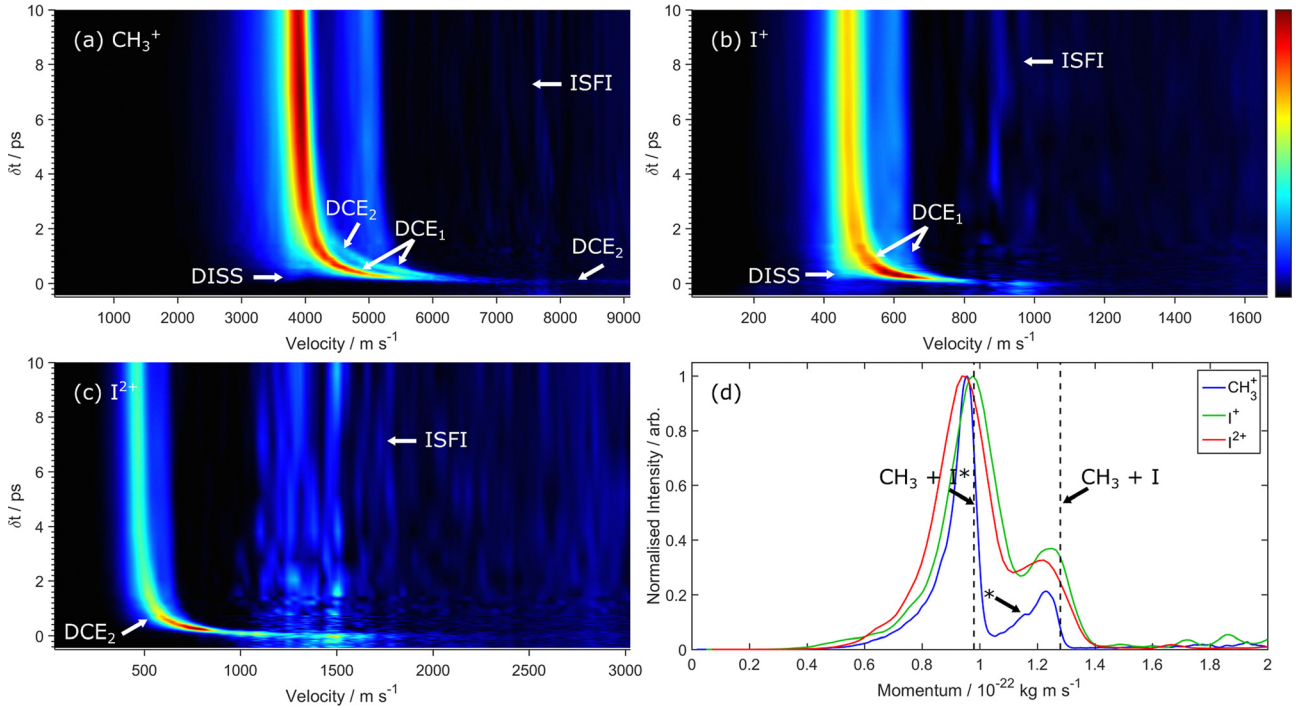

Fig. 13 2-D false-colour maps showing (a) CH_3^+, (b) I^+ and (c) I^{2+} ion velocities as a function of δt obtained by angular integration of the respective images (after appropriate subtraction of the NIR-only contribution) following 267 nm photodissociation of CH_3I and 805 nm SFI probing at $I \sim 1300$ TW cm^{-2}. The data are plotted using the linear false-colour scale shown at the far right of panel (b), and the various channels labelled with the acronyms introduced in the text. (d) Comparison of the $P(p)$ distributions of the CH_3^+, I^+ and I^{2+} ions obtained by integrating data measured over the delay range $0.1 \leq \delta t \leq 1$ ns, with the maximum p values associated with primary photodissociation of $CH_3I(v = 0)$ molecules to form $CH_3(v = 0)$ + I and I* radicals indicated by dashed lines, and the shoulder attributed to formation $CH_3(v_1 = 1)$ + I products marked with an asterisk. Each distribution has been scaled so that the features associated with CH_3 + I* products are shown with the same peak intensity.

the ESI†) the data in which were recorded using significantly lower I by translating the focus of the NIR radiation several mm beyond the point of optimal overlap in the interaction region) show an additional feature at low velocity and $\delta t \sim 0$. This feature, appearing in the presence of both radiation fields, has been interpreted[184,186,207] by assuming that the intense NIR field induces a differential Stark shift of the ground and dissociative excited state potentials, leading to a laser induced conical intersection (LICI) between the transient laser induced potentials (LIPs). Non-adiabatic coupling in the vicinity of this LICI enables flux prepared on the upper LIP (by UV excitation) to propagate towards the (transiently uplifted) lower LIP that correlates with the CH_3 + I asymptote. NIR SFI at extended $H_3C\cdots I$ bond lengths under such conditions then promotes (dissociative) ionisation and formation of the less translationally excited CH_3^+ or I^+ products (together with a neutral co-fragment), yielding the feature labelled LICI in Fig. S9 and S10 (ESI†). Again, the absence of analogous signal in the I^{2+} map reflects the improbability of creating a neutral CH_3 plus I^{2+} product pair under the prevailing conditions.

(ii) XUV/X-ray probing. Two-colour probe studies using FEL-based X-ray photons to induce ionisation have also been reported for CH_3I[67,188,208] and for several other singly and doubly halogenated alkyl halides including 1-iodo-2-methylbutane,[192] 2-iodopropane,[191] CH_2ClI[185] and CH_2BrI.[189,190] These generally employ a probe photon energy above one of the inner shell ionisation thresholds of the iodine atom, which offers much greater initial site specificity and selectivity compared with NIR SFI probe methods. Fig. 15 illustrates the most obvious consequence of this difference by comparing 2D(v, δt) maps of the atomic iodine fragments formed in the 267 nm photolysis of CH_3I, monitored *via* the I^{3+} ion prepared by (a) $\sim$ 120 fs, 108 eV XUV pulses tuned above the I 4d edge and (b) 805 nm SFI with $I = 1300$ TW cm^{-2}. Points to note regarding the XUV probe study[188] include: the I atom is estimated to present an order of magnitude larger photoabsorption cross-section than the CH_3 radical at this probe wavelength (11.5 nm); the observation of I^{q+} ions with $q \leq 4$ implies that multiple ionisations (involving the absorption of at least two XUV photons and subsequent AM decay) occurred under the prevailing experimental conditions; and the CH_3I molecules were pre-aligned using another strong laser field, but this detail is not germane to the present discussion.

Fig. 15(a) is dominated by a constant velocity feature that grows after $\delta t > 0$ and is attributable to site-selective ionisation of primary I photofragments, with no subsequent charge transfer to the geminate CH_3 radical. This signal, the equivalent of the DISS channel in Fig. 11 and 13, reports directly on the neutral C–I bond fission process and yields fragment translational energy distributions consistent with those derived in the earlier ion imaging studies.[204] As Fig. 15(b) and Fig. S6 (ESI†) show, the yield of I^{3+} ions when probing by 805 nm SFI is small, and the probability of forming I^{3+} ions without also ionising the

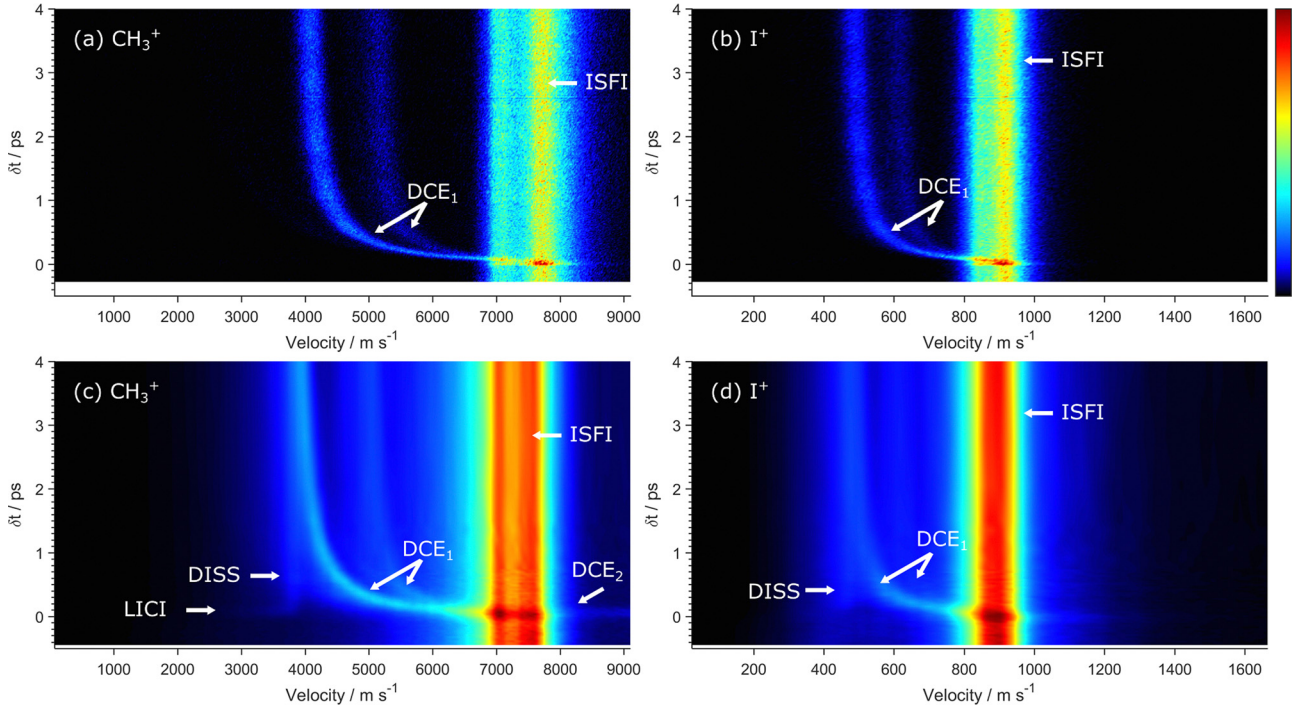

Fig. 14 2-D false-colour maps showing the velocities of (a) CH_3^+ and (b) I^+ ions detected in coincidence, measured over the delay range $-0.28 \leq \delta t \leq 4$ ps, following 263 nm photoexcitation of CH_3I and NIR SFI probing at $I \sim 280$ TW cm^{-2}, with the DISS and DCE_1 product channels labelled. These data are replotted from ref. 187. Panels (c and d) show the corresponding (non-coincident) maps derived from multi-mass imaging measurements employing 267 nm photolysis and NIR SFI probing at $I \sim 650$ TW cm^{-2}, measured over the delay range $-0.45 \leq \delta t \leq 4$ ps (without one-colour background subtraction). The relative intensities in each panel are depicted using the linear false-colour scale shown to the right of panel (b).

geminate CH_3 fragment is essentially non-existent. Thus, the two-colour contribution in Fig. 15(b) is dominated by the dissociative Coulomb explosion component DCE_3, the velocity of which will converge to that of the neutral dissociation products at longer δt. (The corresponding two-colour map without subtraction of the NIR-SFI only contribution is shown in Fig. S11 in the ESI†).

Careful inspection of the DISS signals associated with different I^{q+} products formed by core-ionisation (X-ray probing), like that shown in Fig. 15(a), reveals that their onsets are delayed relative to $\delta t = 0$ and that this delay increases with q.[67,183,188] Such trends can be explained, qualitatively at least, using a classical over-the-barrier model.[67,209] At very early pump–probe delays, the selectively ionised fragment is too close to its geminate partner to prevent inter-fragment charge (electron) transfer and subsequent mutual Coulomb repulsion and acceleration. The barrier to charge transfer increases with increasing inter-fragment separation (*i.e.* with increasing δt) and, at some critical distance, charge transfer to the partner fragment is no longer possible and the DISS signal grows in. This critical distance increases with q, explaining the progressively delayed onset of the DISS feature when probing *via* higher I^{q+} states.

IV. Conclusions and future prospects

As noted at the outset, understanding of the dynamics of molecular photodissociation processes has advanced massively in the past few decades. The photodissociation dynamics of many families of small neutral molecules, including many of key atmospheric and astrochemical interest, have now been characterised experimentally in considerable detail. Theory has shown similarly impressive advances. Given sufficient demand, multi-dimensional excited state PESs can now be calculated with high accuracy for most small/medium sized neutral molecules, as can the non-adiabatic couplings between and the nuclear dynamics on such PESs. Ultrafast laser methods have encouraged the transitioning of such dynamical interests into condensed phase environments, and to studies of photoinduced intramolecular bond fission (*e.g.* ring-opening) reactions.

CEI methods have now entered mainstream contemporary atomic and molecular physics research and are finding ever increasing use as a means of exploring the static stereo-configurations of small quantum systems (molecules, clusters, *etc*), and of tracking the time-evolution of such structures. Based on the examples featured in this Perspective one might argue that CEI methods have 'yet to deliver' penetrating new insights into the photofragmentation dynamics of neutral molecules, but this situation can surely be expected to improve as the technique is applied to a wider range of (larger) molecules, along with greater use of covariance and coincidence analysis methods.[210] The data shown in Fig. 15(a) highlight some of the potential benefits (*e.g.* site selectivity, image simplification) of using X-ray core-ionisation methods to probe molecules in the act of dissociating. As noted in the Introduction, the dynamics of the UV photoinduced ring-

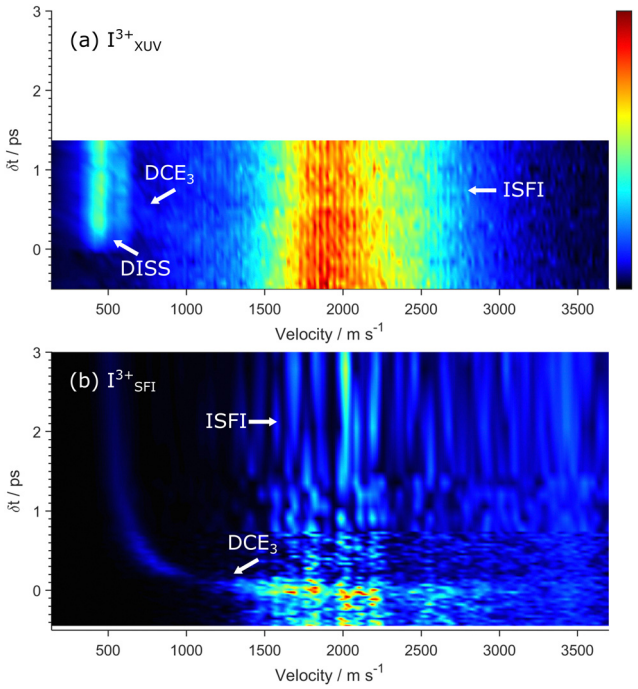

Fig. 15 2-D false-colour maps comparing the I^{3+} ion velocities following 267 nm photolysis of CH_3I and probing with (a) an 11.5 nm XUV pulse and (b) 805 nm SFI with $I \sim 1300$ TW cm^{-2} (after subtraction of the NIR-only contribution), illustrating the very different relative weights of the DISS and DCE_3 signal contributions in the two cases. The relative intensities in both panels are depicted using the linear false-colour scale shown to the right of panel (a).

opening of thiophenone has been explored recently by both time-resolved photoelectron spectroscopy[22] and ultrafast electron diffraction[32] methods. Simulated Newton plots of the H^+ or C^+ fragment momenta, in a plane defined by the O^+ and S^+ atom momenta, suggest that CE methods should provide another route to distinguishing ring-opened and ring-closed photoproducts.

More widely, CEI methods are already providing access to an extraordinarily wide range of multiply charged molecular cations, thereby offering exciting new opportunities to explore the progression from valence-dominated to Coulomb-dominated fragmentation dynamics with increasing charge, and ways in which this varies with molecular size and composition. To date, the body of *ab initio* electronic structure and molecular dynamics calculations for molecular cations, particularly multiply charged molecular cations, is *much* sparser than for neutral systems. Modelling the diverse range of possible fragmentation pathways and dynamics available to multiply charged cations – formed in the presence of a strong laser field – is likely to remain a major challenge for some time to come.

Experimentally, image analyses return particle velocities, and momentum matching arguments built on such measurements are pivotal to understanding many of the fragmentation pathways reported for polyatomic parent cations. Thus far, much less attention has been given to understanding the absolute fragment velocities. One can anticipate that multiply charged parent cations prepared by NIR SFI might be formed in a range of electronic states, and with significant vibrational excitation (due to Raman excitations). NIR pump–probe studies of CH_3I using moderate NIR field strengths[182] lend support to such expectations and for a 'ladder climbing' pumping mechanism[211] wherein higher charge states are accessed by successive promotions *via* parent states of lower charge. The overall time scale could be sufficient to allow some nuclear distortion from the starting geometry *en route* to the final higher charge state. But other NIR SFI studies of CH_3I, at significantly higher field strengths, have returned quite sharp images for all I^{q+} ($q \leq 5$ at least) fragments, implying that each are formed with relatively narrow velocity distributions.[59] Companion (field-free) *ab initio* electronic structure plus trajectory calculations consistently predict substantially higher I^{q+} ($q > 2$) fragment ion velocities than those determined experimentally. This discrepancy has been rationalised by suggesting a role for non-adiabatic coupling and intramolecular charge transfer in the CE of more highly charged CH_3I^{Z+} molecular ions.[59] More studies, preferably coincidence studies that track not just the fragment ion velocities but also those of the ejected photoelectrons would surely help in understanding the fragmentation dynamics of multiply charged parent cations. More generally, as also noted above, ultrafast pump – CEI probe experiments can also be expected to provide a wealth of new insights into charge transfer processes between moieties separating under much greater stereochemical control than achieved hitherto in charge transfer studies involving ion-atom and ion-molecule collisions.

Data availability

All data underpinning hitherto unpublished results from the Bristol group are available at the University of Bristol data repository, data.bris, at https://doi.org/10.5523/bris.1c14gl3i484312c6h6lr4nttz9.

Conflicts of interest

The authors declare no conflict of interest.

Acknowledgements

MNRA and SWC are grateful to EPSRC for funding *via* Programme Grant EP/L005913/1. DR is supported by the Chemical Sciences, Geosciences, and Biosciences Division, Office of Basic Energy Sciences, Office of Science, US Department of Energy under grant no. DE-FG02-86ER13491. MNRA is extremely grateful to the many graduate students, research fellows and academic colleagues who contributed to photofragmentation related research throughout his career in Bristol. We also acknowledge Farzaneh Ziaee, Kasra Amini, Utuq Ablikim, and Rebecca Boll for providing the source data for some of figures in this manuscript.

References

1 S. Chapman, Bakerian lectures-Some phenomena of the upper atmosphere, *Proc. Roy. Soc. (London) A*, 1931, **132**, 353–374.
2 Y. Matsumi and M. Kawasaki, Photolysis of atmospheric ozone in the ultraviolet region, *Chem. Rev.*, 2003, **103**, 4767–4782.
3 G. E. Hall and P. L. Houston, Vector correlations in photodissociation dynamics, *Ann. Rev. Phys. Chem.*, 1989, **40**, 375–405.
4 R. Schinke, *Photodissociation Dynamics*, Cambridge University Press, UK, 1993.
5 W. Domcke and D. R. Yarkony, Role of conical intersections in molecular spectroscopy and photoinduced chemical dynamics, *Ann. Rev. Phys. Chem.*, 2012, **63**, 325–352.
6 B. F. E. Curchod and T. J. Martinez, Ab initio nonadiabatic quantum molecular dynamics, *Chem. Rev.*, 2018, **118**, 3305–3336.
7 M. N. R. Ashfold and S. K. Kim, Non-Born-Oppenheimer effects in molecular photochemistry: an experimental perspective, *Phil. Trans. Roy. Soc. A*, 2022, **380**, 20200376.
8 L. J. Butler and D. M. Neumark, Photodissociation dynamics, *J. Phys. Chem.*, 1996, **100**, 12801–12816.
9 H. Reisler and C. Wittig, Photo-initiated unimolecular reactions, *Ann. Rev. Phys. Chem.*, 1986, **37**, 307–349.
10 P. L. Houston, Correlated photochemistry – The legacy of Doppler, Johann Christian, *Acc. Chem. Res.*, 1989, **22**, 309–314.
11 D. W. Chandler and P. L. Houston, Two-dimensional imaging of state-selected photodissociation products detected by multiphoton ionization, *J. Chem. Phys.*, 1987, **87**, 1445–1447.
12 A. T. J. B. Eppink and D. H. Parker, Velocity map imaging of ions and electrons using electrostatic lenses: Application in photoelectron and photofragment ion imaging of molecular oxygen, *Rev. Sci. Instrum.*, 1997, **68**, 3477–3484.
13 *Imaging in Molecular Dynamics*, ed. B. J. Whitaker, Cambridge University Press, UK, 2003.
14 M. N. R. Ashfold, N. H. Nahler, A. J. Orr-Ewing, O. P. J. Vieuxmaire, R. L. Toomes, T. N. Kitsopoulos, I. A. Garcia, D. A. Chestakov, S. M. Wu and D. H. Parker, Imaging the dynamics of gas phase reactions, *Phys. Chem. Chem. Phys.*, 2006, **8**, 26–53.
15 D. W. Chandler, P. L. Houston and D. H. Parker, Perspective: Advanced particle imaging, *J. Chem. Phys.*, 2017, **147**, 013601.
16 L. Schnieder, W. Meier, K. H. Welge, M. N. R. Ashfold and C. M. Western, Photodissociation dynamics of H_2S at 121.6 nm and a determination of the potential energy function of $SH(A^2\Sigma^+)$, *J. Chem. Phys.*, 1990, **92**, 7027–7037.
17 M. N. R. Ashfold, G. A. King, D. Murdock, M. G. D. Nix, T. A. A. Oliver and A. G. Sage, $\pi\sigma^*$ excited states in molecular photochemistry, *Phys. Chem. Chem. Phys.*, 2010, **12**, 1218–1238.
18 Y. Chang, M. N. R. Ashfold, K. J. Yuan and X. M. Yang, Exploring the vacuum ultraviolet photochemistry of astrochemically important triatomic molecules using a free electron laser, *Nat. Sci. Rev.*, DOI: **10.1093/nsr/nwad158**.
19 A. H. Zewail, Femtochemistry: Atomic-scale dynamics of the chemical bond, *J. Phys. Chem. A*, 2000, **104**, 5660–5694.
20 A. Stolow, A. E. Bragg and D. M. Neumark, Femtosecond time-resolved photoelectron spectroscopy, *Chem. Rev.*, 2004, **104**, 1719–1757.
21 T. Suzuki, Femtosecond time-resolved photoelectron imaging, *Ann. Rev. Phys. Chem.*, 2006, **57**, 555–592.
22 S. Pathak, L. M. Ibele, R. Boll, C. Callegari, A. Demidovich, B. Erk, R. Feifel, R. Forbes, M. Di Fraia, L. Giannessi, C. S. Hansen, D. M. P. Holland, R. A. Ingle, R. Mason, O. Plekan, K. C. Prince, A. Rouzée, R. J. Squibb, J. Tross, M. N. R. Ashfold, B. F. E. Curchod and D. Rolles, Tracking the ultraviolet photochemistry of thiophenone during and after initial ultrafast ring opening, *Nat. Chem.*, 2020, **12**, 795–800.
23 N. Kotsina and D. Townsend, Improved insights into time-resolved photoelectron imaging, *Phys. Chem. Chem. Phys.*, 2021, **23**, 10736–10755.
24 M. S. Schuurman and V. Blanchet, Time-resolved photoelectron spectroscopy: the continuing evolution of a mature technique, *Phys. Chem. Chem. Phys.*, 2022, **24**, 20012–20024.
25 C. A. Rivera, N. Winter, R. V. Harper, I. Benjamin and S. E. Bradforth, The dynamical role of solvent on the ICN photodissociation reaction: connecting experimental observables directly with molecular dynamics simulations, *Phys. Chem. Chem. Phys.*, 2011, **13**, 8269–8283.
26 M. P. Grubb, P. M. Coulter, H. J. B. Marroux, B. Hornung, R. S. McMullen, A. J. Orr-Ewing and M. N. R. Ashfold, Translational, rotational and vibrational relaxation dynamics of a solute molecule in a non-interacting solvent, *Nat. Chem.*, 2016, **8**, 1042–1046.
27 E. H. Choi, Y. Lee, J. Heo and H. Ihee, Reaction dynamics studied via femtosecond X-ray liquidography at X-ray free-electron lasers, *Chem. Sci.*, 2022, **13**, 8457–8490.
28 M. N. R. Ashfold, M. Bain, C. S. Hansen, R. A. Ingle, T. N. V. Karsili, B. Marchetti and D. Murdock, Exploring the dynamics of the photoinduced ring-opening of heterocyclic molecules, *J. Phys. Chem. Lett.*, 2017, **8**, 3440–3451.
29 H. Ihee, V. A. Lobastov, U. M. Gomez, B. M. Goodson, R. Srinivasan, C. Y. Ruan and A. H. Zewail, Direct imaging of transient molecular structures with ultrafast diffraction, *Science*, 2001, **291**, 458–462.
30 T. J. A. Wolf, D. M. Sanchez, J. Yang, R. M. Parrish, J. P. F. Nunes, M. Centurion, R. Coffee, J. P. Cryan, M. Guehr, K. Hegazy, A. Kirrander, R. K. Li, J. Ruddock, X. Shen, T. Vecchione, S. P. Weathersby, P. M. Weber, K. Wilkin, H. Yong, Q. Zheng, X. J. Wang, M. P. Minitti and T. J. Martinez, The photochemical ring-opening of 1,3-cyclohexadiene imaged by ultrafast electron diffraction, *Nat. Chem.*, 2019, **11**, 504–509.
31 M. Zhang, Z. N. Guo, X. Y. Mi, L. Zheng and Y. Q. Liu, Ultrafast imaging of molecular dynamics using ultrafast

low-frequency lasers, X-ray free electron lasers, and electron pulses, *J. Phys. Chem. Lett.*, 2022, **13**, 1668–1680.

32 J. P. F. Nunes, L.-M. Ibele, S. Pathak, A. R. Attar, S. Bhattacharyya, R. Boll, K. Borne, M. Centurion, B. Erk, M.-F. Lin, R. J. G. Forbes, N. Goff, C. S. Hansen, M. Hoffmann, D. M. P. Holland, R. A. Ingle, D. Luo, S. B. Muvva, A. Reid, A. Rouzée, A. Rudenko, S. K. Saha, X. Z. Shen, A. S. Venkatachalam, X. J. Wang, M. R. Ware, S. P. Weathersby, K. Wilkin, T. J. A. Wolf, Y. W. Xiong, J. Yang, M. N. R. Ashfold, D. Rolles and B. F. E. Curchod, Time-dependent quantum yields for a photochemical reaction from ultrafast electron diffraction, *Sci. Adv.*, submitted.

33 A. Odate, A. Kirrander, P. M. Weber and M. P. Minitti, Brighter, faster, stronger: ultrafast scattering of free molecules, *Adv. Phys.: X*, 2023, **8**, 2126796.

34 T. A. Carlson and R. M. White, Measurement of the relative abundances and recoil-energy spectra of fragment ions produced as the initial consequences of X-ray interaction with CH_3I, HI, and DI, *J. Chem. Phys.*, 1966, **44**, 4510.

35 Z. Vager, R. Naaman and E. P. Kanter, Coulomb explosion imaging of small molecules, *Science*, 1989, **244**, 426–431.

36 Z. Vager, Coulomb explosion imaging of molecules, in *Advances in Atomic, Molecular and Optical Physics*, ed. B. Bederson and H. Walther, 2001, vol. 45, pp. 203–239 and references therein.

37 L. J. Frasinski, K. Codling and P. A. Hatherly, Covariance mapping – A correlation method applied to multiphoton multiple ionization, *Science*, 1989, **246**, 1029–1031.

38 K. W. D. Ledingham, R. P. Singhal, D. J. Smith, T. McCanny, P. Graham, H. S. Kilic, W. X. Peng, S. L. Wang, A. J. Langley, P. F. Taday and C. Kosmidis, Behavior of polyatomic molecules in intense infrared laser beams, *J. Phys. Chem. A*, 1998, **102**, 3002–3005.

39 J. L. Xu, C. I. Blaga, P. Agostini and L. F. DiMauro, Time-resolved molecular imaging, *J. Phys. B: At. Mol. Phys.*, 2016, **49**, 112001.

40 T. Yatsuhashi and N. Nakashima, Multiple ionization and Coulomb explosion of molecules, molecular complexes, clusters and solid surfaces, *J. Photochem. Photobiol. C*, 2018, **34**, 52–84 and references therein.

41 C. S. Slater, S. Blake, M. Brouard, A. Lauer, C. Vallance, C. S. Bohun, L. Christensen, J. H. Nielsen, M. P. Johansson and H. Stapelfeldt, Coulomb-explosion imaging using a pixel-imaging mass-spectrometry camera, *Phys. Rev. A*, 2015, **91**, 053424.

42 R. Boll, J. M. Schaefer, B. Richard, K. Fehre, G. Kastirke, Z. Jurek, M. S. Schöffler, M. M. Abdullah, N. Anders, T. M. Baumann, S. Eckart, B. Erk, A. De Fanis, R. Dörner, S. Grundmann, P. Grychtol, A. Hartung, M. Hofmann, M. Ilchen, L. Inhester, C. Janke, R. Jin, M. Kircher, K. Kubicek, M. Kunitski, X. Li, T. Mazza, S. Meister, N. Melzer, J. Montano, V. Music, G. Nalin, Y. Ovcharenko, C. Passow, A. Pier, N. Rennhack, J. Rist, D. E. Rivas, D. Rolles, I. Schlichting, L. P. H. Schmidt, P. Schmidt, J. Siebert, N. Strenger, D. Trabert, F. Trinter, I. Vela-Perez, R. Wagner, P. Walter, M. Weller, P. Ziolkowski, S. K. Son, A. Rudenko, M. Meyer, R. Santra and T. Jahnke, X-ray multiphoton-induced Coulomb explosion images complex single molecules. *Nat. Phys.* 2022, **18**, 423–428.

43 C. A. Schouder, A. S. Chatterley, J. D. Pickering and H. Stapelfeldt, Laser-induced Coulomb explosion imaging of aligned molecules and molecular dimers, *Ann. Rev. Phys. Chem.*, 2022, **73**, 323–347.

44 X. K. Li, X. T. Yu, P. Ma, X. N. Zhao, C. C. Wang, S. Z. Luo and D. J. Ding, Ultrafast Coulomb explosion imaging of molecules and molecular clusters, *Chin. Phys. B*, 2022, **31**, 103304.

45 U. Ablikim, C. Bomme, T. Osipov, H. Xiong, R. Obaid, R. C. Bilodeau, N. G. Kling, I. Dumitriu, S. Augustin, S. Pathak, K. Schnoor, D. Kilcoyne, N. Berrah and D. Rolles, A coincidence velocity map imaging spectrometer for ions and high-energy electrons to study inner-shell photoionization of gas-phase molecules, *Rev. Sci. Instrum.*, 2019, **90**, 055103.

46 S. Pathak, R. Obaid, S. Bhattacharyya, J. Burger, X. Li, J. Tross, T. Severt, B. Davis, R. C. Bilodeau, C. A. Trallero-Herrero, A. Rudenko, N. Berrah and D. Rolles, Differentiating and quantifying gas-phase conformational isomers using Coulomb explosion imaging, *J. Phys. Chem. Lett.*, 2020, **11**, 10205–10211.

47 M. Pitzer, M. Kunitski, A. S. Johnson, T. Jahnke, H. Sann, F. Sturm, L. P. H. Schmidt, H. Schmidt-Böcking, R. Dörner, J. Stohner, J. Kiedrowski, M. Reggelin, S. Marquardt, A. Schiesser, R. Berger and M. S. Schöffler, Direct determination of absolute molecular stereochemistry in gas phase by Coulomb explosion imaging, *Science*, 2013, **341**, 1096–1100.

48 C. Saribal, A. Owens, A. Yachmenev and J. Küpper, Detecting handedness of spatially oriented molecules by Coulomb explosion imaging, *J. Chem. Phys.*, 2021, **154**, 071101.

49 T. Kawaguchi, T. Kitagawa, K. Toyota, M. Kozaki, K. Okada, N. Nakashima and T. Yatsuhashi, Smallest organic tetracation in the gas phase: Stability of multiply charged diiodoacetylene produced in intense femtosecond laser fields, *J. Phys. Chem. A*, 2021, **125**, 8014–8024.

50 M. Li, M. Zhang, O. Vendrell, Z. N. Guo, Q. R. Zhu, X. Gao, L. S. Cao, K. Y. Guo, Q. Q. Su, W. Cao, S. Q. Luo, J. Q. Yan, Y. M. Zhou, Y. Q. Liu, P. X. Lu and Z. Li, Ultrafast imaging of spontaneous symmetry breaking in a photoionized molecular system, *Nat. Commun.*, 2021, **12**, 4233.

51 L. V. Keldysh, Ionization in the field of a strong electromagnetic wave, *Sov. Phys. JETP*, 1965, **20**, 1307–1314.

52 P. B. Corkum, Plasma perspective on strong-field multiphoton ionization, *Phys. Rev. Lett.*, 1993, **71**, 1994–1997.

53 M. Lezius, V. Blanchet, M. Y. Ivanov and A. Stolow, Polyatomic molecules in strong laser fields: Nonadiabatic multielectron dynamics, *J. Chem. Phys.*, 2002, **117**, 1575–1588.

54 A. E. Boguslavskiy, J. Mikosch, A. Gijsbertsen, M. Spanner, S. Patchkovskii, N. Gador, M. J. J. Vrakking and A. Stolow, The multielectron ionization dynamics underlying attosecond strong-field spectroscopies, *Science*, 2012, **335**, 1336–1340.

55 A. Rudenko, L. Inhester, K. Hanasaki, X. Li, S. J. Robatjazi, B. Erk, R. Boll, K. Toyota, Y. Hao, O. Vendrell, C. Bomme,

E. Savelyev, B. Rudek, L. Foucar, S. H. Southworth, C. S. Lehmann, B. Kraessig, T. Marchenko, M. Simon, K. Ueda, K. R. Ferguson, M. Bucher, T. Gorkhover, S. Carron, R. Alonso-Mori, J. E. Koglin, J. Correa, G. J. Williams, S. Boutet, L. Young, C. Bostedt, S.-K. Son, R. Santra and D. Rolles, Femtosecond response of polyatomic molecules to ultra-intense hard X-rays, *Nature*, 2017, **546**, 129–132.

56 D. Rolles, Time-resolved experiments on gas phase atoms and molecules with XUV and X-ray free electron lasers, *Adv. Phys.:X*, 2023, **8**, 2132182 and references therein.

57 D. Matsakis, A. Coster, B. Laster and R. Sime, A renaming proposal: 'The Auger-Meitner effect', *Phys. Today*, 2019, **72**, 10–11.

58 L. J. Frasinski, Covariance mapping techniques, *J. Phys. B: At. Mol. Phys.*, 2016, **49**, 152004.

59 S. W. Crane, L. F. Ge, G. A. Cooper, B. P. Carwithen, M. Bain, J. A. Smith, C. S. Hansen and M. N. R. Ashfold, Non-adiabatic coupling effects in the 800 nm strong field ionization induced Coulomb explosion of methyl iodide revealed by multi-mass velocity map imaging and *ab initio* simulation studies, *J. Phys. Chem. A*, 2021, **125**, 9594–9608.

60 S. W. Crane, J. W. L. Lee and M. N. R. Ashfold, Multi-mass velocity map imaging study of the 805 nm strong field ionization of CF_3I, *Phys. Chem. Chem. Phys.*, 2022, **24**, 18830–18840.

61 W. W. Zhou, L. F. Ge, G. A. Cooper, S. W. Crane, M. H. Evans, M. N. R. Ashfold and C. Vallance, Coulomb explosion imaging for gas-phase molecular structure determination: an *ab initio* trajectory simulation study, *J. Chem. Phys.*, 2020, **153**, 184201.

62 J. H. D. Eland, R. Feifel and M. Hochlaf, Double photoionization and dication fragmentation of CF_3I: Experiment and theory, *J. Chem. Phys.*, 2008, **128**, 234303.

63 M. E. Corrales, G. Gitzinger, J. González-Vázquez, V. Loriot, R. de Nalda and L. Bañares, Velocity map imaging and theoretical study of the Coulomb explosion of CH_3I under intense femtosecond IR pulses, *J. Phys. Chem. A*, 2012, **116**, 2669–2677.

64 D. D. Zhang, S. Z. Luo, H. F. Xu, X. M. Jin, F. C. Liu, B. Yan, Z. G. Wang, H. Liu, D. W. Jiang, A. Eppink, W. Roeterdink, S. Stolte and D. J. Ding, Dissociative ionization and Coulomb explosion of CH_3I in intense femtosecond laser fields, *Eur. Phys. J. D*, 2017, **71**, 148.

65 A. Sen, S. Mandal, S. Sen, B. Bapat, R. Gopal and V. Sharma, Dissociation dynamics of multiply charged CH_3I in moderately intense laser fields, *Phys. Rev. A*, 2021, **103**, 043107.

66 K. Motomura, E. Kukk, H. Fukuzawa, S. Wada, K. Nagaya, S. Ohmura, S. Mondal, T. Tachibanai, Y. Ito, R. Koga, T. Sakai, K. Matsunami, A. Rudenko, C. Nicolas, X.-J. Liu, C. Miron, Y. Z. Zhang, Y. H. Jiang, J. H. Chen, M. Anandl, D. E. Kim, K. Tono, M. Yabashi, M. Yao and K. Ueda, Charge and nuclear dynamics induced by deep inner shell multiphoton ionization of CH_3I molecules by intense X-ray free-electron laser pulses, *J. Phys. Chem. Lett.*, 2015, **6**, 2944–2949.

67 B. Erk, R. Boll, S. Trippel, D. Anielski, L. Foucar, B. Rodek, S. W. Epp, R. Coffee, S. Carron, S. Schorb, K. R. Ferguson, M. Swiggers, J. D. Bozek, M. Simon, T. Marchenko, J. Küpper, I. Schlichting, J. Ullrich, C. Bostedt, D. Rolles and A. Rudenko, Imaging charge transfer in iodomethane upon X-ray photoabsorption, *Science*, 2014, **345**, 288–291.

68 H. K. Woo, P. Wang, K.-C. Lau, X. Xing and C. Y. Ng, Vacuum ultraviolet (VUV) pulsed field ionization - photoelectron and VUV-IR photoinduced Rydberg ionization study of *trans*-dichloroethene, *J. Phys. Chem. A*, 2004, **108**, 9637–9644.

69 K.-C. Lau, H. K. Woo, P. Wang, X. Xing and C. Y. Ng, Vacuum ultraviolet laser pulsed field ionization-photoelectron study of *cis*-dichloroethene, *J. Chem. Phys.*, 2006, **124**, 224311.

70 I. Powis, R. C. Menzies, D. M. P. Holland, A. B. Trofimov, A. D. Skitnevskaya, E. V. Gromov, E. Antonsson, M. Patanen, C. Nicolas and C. Miron, Photoionization dynamics of *cis*-dichloroethene from investigation of vibronically resolved photoelectron spectra and angular distributions, *J. Chem. Phys.*, 2018, **149**, 074305.

71 A. B. Trofimov, I. Powis, R. C. Menzies, D. M. P. Holland, E. Antonsson, M. Patanen, C. Nicolas, C. Miron, A. D. Skitnevskaya, E. V. Gromov and H. Köppel, An experimental and theoretical study of the photoelectron spectra of *cis*-dichloroethene: Valence shell vertical ionization and vibronic coupling in the low-lying cationic states, *J. Chem. Phys.*, 2018, **149**, 074306.

72 A. T. Duran, I. Powis, D. M. P. Holland, C. Nicolas, J. Bozek, A. B. Trofimov, E. K. Grigoricheva and A. D. Skitnevskaya, Vibronic interaction in *trans*-dichloroethene studied by vibration- and angle-resolved photoelectron spectroscopy using 19–90 eV photon energy, *J. Chem. Phys.*, 2021, **154**, 094303.

73 M. A. Parkes, S. Ali, C. R. Howle, R. P. Tuckett and A. E. R. Malins, The photoionization dynamics of the three structural isomers of dichloroethene, *Mol. Phys.*, 2007, **105**, 907–916.

74 A. Bodi, W. R. Stevens and T. Baer, Understanding the complex dissociation dynamics of energy selected dichloroethylene ions: Neutral isomerization energies and heats of formation by imaging photoelectron-photoion coincidence, *J. Phys. Chem. A*, 2011, **115**, 726–734.

75 N. Kishimoto and Y. Nishi, An automated exploration of the isomerization and dissociation pathways of (*E*)-1,2-dichloroethene cations and anions, *Chem. Phys. Lett.*, 2017, **674**, 77–85.

76 J. Roithová, J. Hrušák and Z. Herman, A theoretical study of the ground and excited states of the $CHCl^{2+}$ dication and the $CHCl^{+}$ cation, *Int. J. Mass Spectrom.*, 2003, **228**, 497–506.

77 J. Roithová, J. Žabka, R. Thissen and Z. Herman, Dynamics of chemical and charge-transfer reactions of molecular dications, *Phys. Chem. Chem. Phys.*, 2003, **5**, 2988–2995.

78 J. Jašík and J. Roithová, Infrared spectroscopy of $CHCl^{2+}$ molecular cations, *Int. J. Mass Spectrom.*, 2015, **377**, 109–115.

79 U. Ablikim, C. Bomme, H. Xiong, E. Savelyev, R. Obaid, B. Kaderiya, S. Augustin, K. Schnorr, I. Dumitriu, T. Osipov, R. Bilodeau, D. Kilcoyne, V. Kumarappan, A. Rudenko, N. Berrah and D. Rolles, Identification of absolute geometries of *cis* and *trans* molecular isomers by Coulomb explosion imaging, *Sci. Rep.*, 2016, **6**, 38202.

80 U. Ablikim, *Coulomb explosion imaging of polyatomic molecules after photoionization with X-rays and strong laser fields*, PhD thesis, Kansas State University, 2017.

81 J. Rajput, T. Severt, B. Berry, B. Jochim, P. Feizollah, B. Kaderiya, M. Zohrabi, U. Ablikim, F. Ziaee, P. K. Raju, D. Rolles, A. Rudenko, K. D. Carnes, B. D. Esry and I. Ben-Itzhak, Native frames: Disentangling sequential from concerted three-body fragmentation, *Phys. Rev. Lett.*, 2018, **120**, 103001.

82 S. Pathak, R. Obaid, S. Bhattacharyya, J. Bürger, X. Li, J. Tross, T. Severt, B. Davis, R. C. Bilodeau, C. A. Trallero-Herrero, A. Rudenko, N. Berrah and D. Rolles, Differentiating and quantifying gas-phase conformational isomers using Coulomb explosion imaging, *J. Phys. Chem. Lett.*, 2020, **11**, 10205–10211.

83 J. W. McManus, T. Walmsley, K. Nagaya, J. R. Harries, Y. Kumagai, H. Iwayama, M. N. R. Ashfold, M. Britton, P. H. Bucksbaum, B. Downes-Ward, T. Driver, D. Heatcote, P. Hockett, A. J. Howard, E. Kukk, J. W. L. Lee, Y. S. Liu, D. Milesevic, R. S. Minns, A. Niozu, J. Niskanen, A. J. Orr-Ewing, S. Owada, D. Rolles, P. A. Robertson, A. Rudenko, K. Ueda, J. Unwin, C. Vallance, M. Burt, M. Brouard, R. Forbes and F. Allum, Disentangling sequential and concerted fragmentations of molecular polycations with covariant native frame analysis, *Phys. Chem. Chem. Phys.*, 2022, **24**, 22699–22709.

84 S. Bhattacharyya, K. Borne, F. Ziaee, S. Pathak, E. L. Wang, A. S. Venkatachalam, N. Marshall, K. D. Carnes, C. W. Fehrenbach, T. Severt, I. Ben-Itzhak, A. Rudenko and D. Rolles, Two- and three-body fragmentation of multiply charged tribromomethane by ultrafast laser pulses, *Phys. Chem. Chem. Phys.*, 2022, **24**, 27631–27644.

85 I. Luzon, E. Livshits, K. Gope, R. Baer and D. Strasser, Making sense of Coulomb explosion imaging, *J. Phys. Chem. Lett.*, 2019, **10**, 1361–1367.

86 J. W. L. Lee, H. Kockert, D. Heathcote, D. Popat, R. T. Chapman, G. Karras, P. Majchrzak, E. Springate and C. Vallance, Three-dimensional covariance-map imaging of molecular structure and dynamics on the ultrafast timescale, *Comm. Chemun.*, 2020, **3**, 72.

87 D. M. Bittner, K. Gope, E. Livshits, R. Baer and D. Strasser, Sequential and concerted C–C and C–O bond dissociation in the Coulomb explosion of 2-propanol, *J. Chem. Phys.*, 2022, **157**, 074309.

88 B. Jochim, L. De Jesus and M. Dantus, Ultrafast disruptive probing: Simultaneously keeping track of tens of reaction pathways, *Rev. Sci. Instrum.*, 2022, **93**, 033003.

89 J. H. Sanderson, A. El-Zein, W. A. Bryan, W. R. Newell, A. J. Langley and P. F. Taday, Geometry modifications and alignment of H_2O in an intense femtosecond laser pulse, *Phys. Rev. A*, 1999, **59**, R2567–R2570.

90 S. Zhao, B. Jochim, P. Feizollah, J. Rajput, F. Ziaee, P. K. Raju, B. Kaderiya, K. Borne, Y. Malakar, B. Berry, J. Harrington, D. Rolles, A. Rudenko, K. D. Carnes, E. Wells, I. Ben-Itzhak and T. Severt, Strong-field-induced bond rearrangement in triatomic molecules, *Phys. Rev. A*, 2019, **99**, 053412.

91 A. J. Howard, C. Cheng, R. Forbes, G. A. McCracken, W. H. Mills, V. Makhija, M. Spanner, T. Weinacht and P. H. Bucksbaum, Strong-field ionization of water: Nuclear dynamics revealed by varying the pulse duration, *Phys. Rev. A*, 2021, **103**, 043120.

92 C. Cheng, Z. L. Streeter, A. J. Howard, M. Spanner, R. R. Lucchese, C. W. McCurdy, T. Weinacht, P. H. Bucksbaum and R. Forbes, Strong-field ionization of water. II. Electronic and nuclear dynamics en route to double ionization, *Phys. Rev. A*, 2021, **104**, 023108.

93 T. Severt, Z. L. Streeter, W. Iskandar, K. A. Larsen, A. Gatton, D. Trabert, B. Jochim, B. Griffin, E. G. Champenois, M. M. Brister, D. Reedy, D. Call, R. Strom, A. L. Landers, R. Dörner, J. B. Williams, D. S. Slaughter, R. R. Luchesse, T. Weber, C. W. McCurdy and I. Ben-Itzhak, Step-by-step state-selective tracking of fragmentation dynamics of water dications by momentum imaging, *Nat. Commun.*, 2022, **13**, 5146.

94 T. Jahnke, R. Guillemin, L. Inhester, S. K. Son, G. Kastirke, M. Ilchen, J. Rist, D. Trabert, N. Melzer, N. Anders, T. Mazza, R. Boll, A. De Fanis, V. Music, T. Weber, M. Weller, S. Eckart, K. Fehre, S. Grundmann, A. Hartung, M. Hofmann, C. Janke, M. Kircher, G. Nalin, A. Pier, J. Siebert, N. Strenger, I. Vela-Perez, T. M. Baumann, P. Grychtol, J. Montano, Y. Ovcharenko, N. Rennhack, D. E. Rivas, R. Wagner, P. Ziolkowski, P. Schmidt, T. Marchenko, O. Travnikova, L. Journel, I. Ismael, E. Kukk, J. Niskanen, F. Trinter, C. Vozzi, M. Devetta, S. Stagira, M. Gisselbrecht, A. L. Jager, X. Li, Y. Malakar, M. Martins, R. Feifel, L. P. H. Schmidt, A. Czasch, G. Sansone, D. Rolles, A. Rudenko, R. Moshammer, R. Dorner, M. Meyer, T. Pfeifer, M. S. Schoffler, R. Santra, M. Simon and M. N. Piancastelli, Inner-shell-ionization-induced femtosecond structural dynamics of water molecules imaged at an X-ray free-electron laser, *Phys. Rev. X*, 2021, **11**, 041044.

95 A. Hishikawa, E. J. Takahashi and A. Matsuda, Electronic and nuclear responses of fixed-in-space H_2S to ultrashort intense laser fields, *Phys. Rev. Lett.*, 2006, **97**, 243002.

96 C. Cornaggia, M. Schmidt and D. Normand, Coulomb explosion of CO_2 in an intense femtosecond laser field, *J. Phys. B., At. Mol. Opt. Phys.*, 1994, **27**, L123–L130.

97 A. Hishikawa, A. Iwamae and K. Yamanouchi, Ultrafast deformation of the geometrical structure of CO_2 induced in intense laser fields, *Phys. Rev. Lett.*, 1999, **83**, 1127–1130.

98 W. A. Bryan, J. H. Sanderson, A. El-Zein, W. R. Newell, P. F. Taday and A. J. Langley, Laser-induced Coulomb explosion, geometry modification and reorientation of carbon dioxide, *J. Phys. B: At. Mol. Phys.*, 2000, **33**, 745–766.

99 K. Zhao, G. Zhang and W. T. Hill, Strong-field dissociative ionization of a linear triatomic molecule: Relationship

between Coulomb-explosion energies and bond angle, *Phys. Rev. A*, 2003, **68**, 063408.

100 K. Zhao and W. T. Hill, Ejection anisotropy in three-atom Coulomb explosions, *Phys. Rev. A*, 2005, **71**, 013412.

101 J. P. Brichta, S. J. Walker, R. Helsten and J. H. Sanderson, Ultrafast imaging of multielectronic dissociative ionization of CO_2 in an intense laser field, *J. Phys. B: At. Mol. Phys.*, 2007, **40**, 117–129.

102 I. Bocharova, R. Karimi, E. F. Penka, J.-P. Brichta, P. Lassonde, X. Q. Fu, J.-C. Kieffer, A. D. Bandrauk, I. Litvinyuk, J. Sanderson and F. Légaré, Charge resonance enhanced ionization of CO_2 probed by laser Coulomb explosion imaging, *Phys. Rev. Lett.*, 2011, **107**, 063201.

103 C. Wu, C. Y. Wu, D. Song, H. M. Su, Y. D. Yang, Z. F. Wu, X. R. Liu, H. Liu, M. Li, Y. K. Deng, Y. Q. Liu, L.-Y. Peng, H. B. Jiang and Q. H. Gong, Nonsequential and sequential fragmentation of CO_2^{3+} in intense laser fields, *Phys. Rev. Lett.*, 2013, **110**, 103601.

104 T. Endo, H. Fujise, A. Matsuda, M. Fushitani, H. Kono and A. Hishikawa, Coincidence momentum imaging of asymmetric Coulomb explosion of CO_2 in phase-locked two-color intense laser fields, *J. Electron Spectrosc. Relat. Phenom.*, 2016, **207**, 50–54.

105 C. Y. Wu, C. Wu, Y. M. Fan, X. G. Xie, P. Wang, Y. K. Deng, Y. Q. Liu and Q. H. Gong, Three-body fragmentation of CO_2 driven by intense laser pulses, *J. Chem. Phys.*, 2015, **142**, 124303.

106 T. Endo, H. Fujise, Y. Kawachi, A. Ishihara, A. Matsuda, M. Fushitani, H. Kono and A. Hishikawa, Selective bond breaking of CO_2 in phase-locked two-color intense laser fields: laser field intensity dependence, *Phys. Chem. Chem. Phys.*, 2017, **19**, 3550–3556.

107 D. M. Bittner, K. Gope and D. Strasser, Time-resolved dissociative ionization and double photoionization of CO_2, *J. Chem. Phys.*, 2020, **153**, 194201.

108 J. H. Sanderson, T. R. J. Goodworth, A. El-Zein, W. A. Bryan, W. R. Newell, A. J. Langley and P. F. Taday, Coulombic and pre-Coulombic geometry evolution of carbonyl sulfide in an intense femtosecond laser pulse, determined by momentum imaging, *Phys. Rev. A*, 2002, **65**, 043403.

109 B. Wales, E. Bisson, R. Karimi, S. Beaulieu, A. Ramadhan, M. Giguère, Z. J. Long, W.-K. Liu, J.-C. Kieffer, F. Légaré and J. Sanderson, Coulomb imaging of the concerted and stepwise break up processes of OCS ions in intense femtosecond laser radiation, *J. Electron Spectrosc. Relat. Phenom.*, 2014, **195**, 332–336.

110 P. Ma, C. C. Wang, S. Z. Luo, X. T. Yu, X. K. Li, Z. Z. Wang, W. H. Hu, J. Q. Yu, Y. Z. Yang, X. Tian, Z. H. Cui and D. J. Ding, Comparison study for multiple ionization of carbonyl sulfide by linearly and circularly polarized intense femtosecond laser fields using Coulomb explosion imaging, *J. At. Mol. Phys. B*, 2018, **51**, 094002.

111 P. Ma, C. C. Wang, S. Z. Luo, X. K. Li, W. H. Hu, J. Q. Yu, X. T. Yu, X. Tian, Z. X. Qu and D. J. Ding, Bond-breakage-dependent dissociative ionization of an asymmetric molecule in an intense femtosecond laser field, *Phys. Rev. A*, 2019, **99**, 023423.

112 T. Endo, K. M. Ziems, M. Richter, F. G. Fröbel, A. Hishikawa, S. Gräfe, F. Légaré and H. Ibrahim, Post-ionization dynamics of the polar molecule OCS in asymmetric laser fields, *Front. Chem.*, 2022, **10**, 859750.

113 H. Hasegawa, A. Hishikawa and K. Yamanouchi, Coincidence imaging of Coulomb explosion of CS_2 in intense laser fields, *Chem. Phys. Lett.*, 2001, **349**, 57–63.

114 A. Hishikawa, H. Hasegawa and K. Yamanouchi, Sequential three-body Coulomb explosion of CS_2 in intense laser fields appearing in momentum correlation map, *Chem. Phys. Lett.*, 2002, **361**, 245–250.

115 A. Hishikawa, H. Hasegawa and K. Yamanouchi, Nuclear dynamics on the light-dressed potential energy surface of CS_2 by coincidence momentum imaging, *Chem. Phys. Lett.*, 2004, **388**, 1–6.

116 A. Hishikawa, M. Ueyama and K. Yamanouchi, Probing the ultrafast nuclear motion in CS_2^{2+} in intense laser fields, *J. Chem. Phys.*, 2005, **122**, 151104.

117 A. Matsuda, E. J. Takahashi and A. Hishikawa, Time-resolved laser Coulomb explosion imaging using few-cycle intense laser pulses: Application to exploding CS_2 in highly charged states, *J. Electr. Spectrosc. Rel. Phenom*, 2014, **195**, 327–331.

118 X. Wang, J. Zhang, S. A. Zhang and Z. R. Sun, Coulomb explosion of CS_2 molecule under an intense femtosecond laser field, *Chin. Phys. B*, 2016, **25**, 053301.

119 A. Matsuda, E. J. Takahashi and A. Hishikawa, Dalitz plot analysis of Coulomb exploding O_3 in ultrashort intense laser fields, *J. Chem. Phys.*, 2007, **127**, 114318.

120 F. Légaré, K. F. Lee, I. V. Litvinyuk, P. W. Dooley, A. D. Bandrauk, D. M. Villeneuve and P. B. Corkum, Imaging the time-dependent structure of a molecule as it undergoes dynamics, *Phys. Rev. A*, 2005, **72**, 052717.

121 M. Ueyama, H. Hasegawa, A. Hishikawa and K. Yamanouchi, Concerted and sequential Coulomb explosion processes of N_2O in intense laser fields by coincidence momentum imaging, *J. Chem. Phys.*, 2005, **123**, 154305.

122 W. B. Jiang, X. C. Wang, S. Zhang, R. C. Dong, Y. L. Guo, J. Z. Feng, Z. J. Shen, T. M. Yan, Z. Y. Zhu and Y. H. Jiang, Dissociative multi-ionization of N_2O molecules in strong femtosecond laser field, *J. Chem. Phys.*, 2022, **157**, 084302.

123 A. Hishikawa, A. Iwamae and K. Yamanouchi, Ultrafast structural deformation of NO_2 in intense laser fields studied by mass-resolved momentum imaging, *J. Chem. Phys.*, 1999, **111**, 8871–8878.

124 A. S. Alnaser, I. Litvinyuk, T. Osipov, B. Ulrich, A. Landers, E. Wells, C. M. Maharjan, P. Ranitovic, I. Bochareva, D. Ray and C. L. Cocke, Momentum-imaging investigations of the dissociation of D_2^+ and the isomerization of acetylene to vinylidene by intense short laser pulses, *J. Phys. B: At. Mol. Phys.*, 2006, **39**, S485–S492.

125 A. Hishikawa, A. Matsuda, M. Fushitani and E. J. Takahashi, Visualizing recurrently migrating hydrogen in acetylene dication by intense ultrashort laser pulses, *Phys. Rev. Lett.*, 2007, **99**, 258302.

126 A. Hishikawa, A. Matsuda, E. J. Takahashi and M. Fushitani, Acetylene-vinylidene isomerization in

ultrashort intense laser fields studied by triple ion-coincidence momentum imaging, *J. Chem. Phys.*, 2008, **128**, 084302.

127 A. Matsuda, M. Fushitani, E. J. Takahashi and A. Hishikawa, Visualizing hydrogen atoms migrating in acetylene dication by time-resolved three-body and four-body Coulomb explosion imaging, *Phys. Chem. Chem. Phys.*, 2011, **13**, 8697–8704.

128 H. Ibrahim, B. Wales, S. Beaulieu, B. E. Schmidt, N. Thire, E. P. Fowe, E. Bisson, C. T. Hebeisen, V. Wanie, M. Giguere, J.-C. Kieffer, M. Spanner, A. D. Bandrauk, M. S. Schuurman, J. Sanderson and F. Légaré, Tabletop imaging of structural evolutions in chemical reactions demonstrated for the acetylene cation, *Nat. Commun.*, 2014, **5**, 4422.

129 S. Miura, T. Ando, K. Ootaka, A. Iwasaki, H. L. Xu, T. Okino, K. Yamanouchi, D. Hoff, T. Rathje, G. G. Paulus, M. Kitzler, A. Baltuska, G. Sansone and M. Nisoli, Carrier-envelope-phase dependence of asymmetric C − D bond breaking in C_2D_2 in an intense few-cycle laser field, *Chem. Phys. Lett.*, 2014, **595**, 61–66.

130 C. Burger, N. G. Kling, R. Siemering, A. S. Alnaser, B. Bergues, A. M. Azzeer, R. Moshammer, R. de Vivie-Riedle, M. Kübel and M. F. Kling, Visualization of bond rearrangements in acetylene using near single-cycle laser pulses, *Farad. Discuss*, 2016, **194**, 495–508.

131 H. T. Hu, Y. Hung, S. Larimian, S. Erattupuzha, A. Baltuska, M. Zeiler and X. H. Xie, Laser-induced valence electron excitation in acetylene, *Front. Phys.*, 2022, **10**, 1076671.

132 C.-M. Tseng, M. Fushitani, A. Matsuda and A. Hishikawa, Coincidence momentum imaging of four- and three-body Coulomb explosion of formaldehyde in ultrashort intense laser fields, *J. Electron Spectrosc. Relat. Phenom.*, 2018, **228**, 25–30.

133 C. Cheng, L. J. Frasinski, G. Moǧol, F. Allum, A. J. Howard, D. Rolles, P. H. Bucksbaum, M. Brouard, R. Forbes and T. Weinacht, Multiparticle cumulant mapping for Coulomb explosion imaging, *Phys. Rev. Lett.*, 2023, **130**, 093001.

134 J. Strohaber, F. Zhu, A. A. Kolomenskii and H. A. Schuessler, Observation of anisotropic fragmentation in methane subjected to femtosecond radiation, *Phys. Rev. A*, 2014, **89**, 023430.

135 P. Ma, C. C. Wang, X. K. Li, X. T. Yu, X. Tian, W. H. Hu, J. Q. Yu, S. Z. Luo and D. J. Ding, Ultrafast proton migration and Coulomb explosion of methyl chloride in intense laser fields, *J. Chem. Phys.*, 2017, **146**, 244305.

136 Y. M. Wang, S. Zhang, Z. R. Wei and B. Zhang, Velocity map imaging of dissociative ionization and Coulomb explosion of CH_3I induced by a femtosecond laser, *J. Phys. Chem. A*, 2008, **112**, 3846–3851.

137 A. Sen, S. Mandal, S. Sen, B. Bapat, R. Copal and V. Sharma, Dissociation dynamics of multiply charged CH_3I in moderately intense laser fields, *Phys. Rev. A*, 2021, **103**, 043107.

138 Y. C. Cheng, B. Oostenrijk, J. Lahl, S. Maclot, S. Augustin, G. Schmid, K. Schnorr, S. Meister, D. Rompotis, B. Manschwetus, H. Redlin, C. Bomme, B. Erk, D. Rolles, R. Boll, P. Olshin, A. Rudenko, M. Meyer, P. Johnsson, R. Moshammer and M. Gisselbrecht, Imaging multiphoton ionization dynamics of CH_3I at a high repetition rate XUV free-electron laser, *J. Phys. B: At. Mol. Phys.*, 2021, **54**, 014001.

139 S. Bhattacharyya, K. Borne, F. Ziaee, S. Pathak, E. L. Wang, A. S. Venkatachalam, X. Li, N. Marshall, K. D. Carnes, C. W. Fehrenbach, T. Severt, I. Ben-Itzhak, A. Rudenko and D. Rolles, Strong-field-induced Coulomb explosion imaging of tribromomethane, *J. Phys. Chem. Lett.*, 2022, **13**, 5845–5853.

140 C. Wang, B. Wang, M. Okunishi, W. G. Roeterdink, D. Ding, R. Zhu, G. Prümper, K. Shimada and K. Ueda, Ion-ion coincidence imaging of dissociative ionization dynamics of formic acid in intense laser fields, *Chem. Phys.*, 2014, **430**, 40–46.

141 T. Severt, D. R. Daugaard, T. Townsend, F. Ziaee, K. Borne, S. Bhattacharyya, K. D. Carnes, D. Rolles, A. Rudenko, E. Wells and I. Ben-Itzhak, Two-body dissociation of formic acid following double ionization by ultrafast laser pulses, *Phys. Rev. A*, 2022, **105**, 053112.

142 X. H. Xie, S. Roither, M. Schoeffler, E. Loetstedt, D. Kartashov, L. Zhang, G. G. Paulus, A. Iwasaki, A. Baltuska, K. Yamanouchi and M. Kitzler, Electronic predetermination of ethylene fragmentation dynamics, *Phys. Rev. X*, 2014, **4**, 021005.

143 Y. Furukawa, K. Hoshina, K. Yamanouchi and H. Nakano, Ejection of triatomic hydrogen molecular ion from methanol in intense laser fields, *Chem. Phys. Lett.*, 2005, **414**, 117–121.

144 T. Okino, Y. Furukawa, P. Liu, T. Ichikawa, R. Itakura, K. Hoshina, K. Yamanouchi and H. Nakano, Coincidence momentum imaging of ejection of hydrogen molecular ions from methanol in intense laser fields, *Chem. Phys. Lett.*, 2006, **419**, 223–227.

145 P. Liu, T. Okino, Y. Furukawa, T. Ichikawa, R. Itakura, K. Hoshina, K. Yamanouchi and H. Nakano, Three-body sequential Coulomb explosions of CH_3OD^{3+} induced by intense laser fields, *Chem. Phys. Lett.*, 2006, **423**, 187–191.

146 T. Okino, Y. Furukawa, P. Liu, T. Ichikawa, R. Itakura, K. Hoshina, K. Yamanouchi and H. Nakano, Coincidence momentum imaging of ultrafast hydrogen migration in methanol and its isotopomers in intense laser fields, *Chem. Phys. Lett.*, 2006, **423**, 220–224.

147 R. Itakura, P. Liu, Y. Furukawa, T. Okino, K. Yamanouchi and H. Nakano, Two-body Coulomb explosion and hydrogen migration in methanol induced by intense 7 and 21 fs laser pulses, *J. Chem. Phys.*, 2007, **127**, 104306.

148 H. L. Xu, T. Okino, T. Kudou, K. Yamanouchi, S. Roither, M. Kitzler, A. Baltuska and S.-L. Chin, Effect of laser parameters on ultrafast hydrogen migration in methanol studied by coincidence momentum imaging, *J. Phys. Chem. A*, 2012, **116**, 2686–2690.

149 T. Ando, A. Shimamoto, S. Miura, K. Nakai, H. L. Xu, A. Iwasaki and K. Yamanouchi, Wave packet bifurcation in ultrafast hydrogen migration in CH_3OH^+ by pump–

probe coincidence momentum imaging with few-cycle laser pulses, *Chem. Phys. Lett.*, 2015, **624**, 78–82.

150 N. Ekanayake, M. Nairat, B. Kaderiya, P. Feizollah, B. Jochim, T. Severt, B. Berry, P. K. Raju, K. D. Carnes, S. Pathak, D. Rolles, A. Rudenko, I. Ben-Itzhak, C. A. Mancuso, B. S. Fales, J. E. Jackson, B. G. Levine and M. Dantus, Mechanisms and time-resolved dynamics for trihydrogen cation (H_3^+) formation from organic molecules in strong laser fields, *Sci. Rep.*, 2017, **7**, 4703.

151 N. Ekanayake, T. Severt, M. Nairat, N. P. Weingartz, B. M. Farris, B. Kaderiya, P. Feizollah, B. Jochim, F. Ziaee, K. Borne, P. K. Raju, K. D. Carnes, D. Rolles, A. Rudenko, B. G. Levine, J. E. Jackson, I. Ben-Itzhak and M. Dantus, H_2 roaming chemistry and the formation of H_3^+ from organic molecules in strong laser fields, *Nat. Commun.*, 2018, **9**, 5186.

152 I. Luzon, K. Jagtap, E. Livshits, O. Lioubashevski, R. Baer and D. Strasser, Single-photon Coulomb explosion of methanol using broad bandwidth ultrafast EUV pulses, *Phys. Chem. Chem. Phys.*, 2017, **19**, 13488–13495.

153 B. Erk, D. Rolles, L. Foucar, B. Rudek, S. W. Epp, M. Cryle, C. Bostedt, S. Schorb, J. Bozek, A. Rouzee, A. Hundertmark, T. Marchenko, M. Simon, F. Filsinger, L. Christensen, S. De, S. Trippel, J. Küpper, H. Stapelfeldt, S. Wada, K. Ueda, M. Swiggers, M. Messerschmidt, C. D. Schröter, R. Moshammer, I. Schlichting, J. Ullrich and A. Rudenko, Ultrafast charge rearrangement and nuclear dynamics upon inner-shell multiple ionization of small polyatomic molecules, *Phys. Rev. Lett.*, 2013, **110**, 053003.

154 A. Hishikawa, H. Hasegawa and K. Yamanouchi, Hydrogen migration in acetonitrile in intense laser fields studied by coincidence momentum imaging, *Phys. Scripta*, 2004, **T110**, 108–111.

155 A. Hishikawa, H. Hasegawa and K. Yamanouchi, Hydrogen migration in acetonitrile in intense laser fields in competition with two-body Coulomb explosion, *J. Electron Spectrosc. Relat. Phenom.*, 2004, **141**, 195–200.

156 M. McDonnell, A. C. LaForge, J. Reino-Gonzalez, M. Disla, N. G. Kling, D. Mishra, R. Obaid, M. Sundberg, V. Svoboda, T. Díaz-Tendero, F. Martin and N. Berrah, Ultrafast laser-induced isomerization dynamics in acetonitrile, *J. Phys. Chem. Lett.*, 2020, **11**, 6724–6729.

157 G. A. Cooper, T. Alavi, W. Li, S. K. Lee and A. G. Suits, Coulomb explosion dynamics of chlorocarbonylsulfenyl chloride, *J. Phys. Chem. A*, 2021, **125**, 5481–5489.

158 H. L. Xu, T. Okino and K. Yamanouchi, Ultrafast hydrogen migration in allene in intense laser fields: Evidence of two-body Coulomb explosion, *Chem. Phys. Lett.*, 2009, **469**, 255–260.

159 H. L. Xu, T. Okino and K. Yamanouchi, Tracing ultrafast hydrogen migration in allene in intense laser fields by triple-ion coincidence momentum imaging, *J. Chem. Phys.*, 2009, **131**, 151102.

160 H. L. Xu, T. Okino and K. Yamanouchi, Ultrafast delocalization of hydrogen atoms in allene in intense laser fields, *Appl. Phys. A: Mater. Sci. Process.*, 2012, **104**, 941–945.

161 T. Okino, A. Watanabe, H. L. Xu and K. Yamanouchi, Ultrafast hydrogen scrambling in methylacetylene and methyl-d_3-acetylene ions induced by intense laser fields, *Phys. Chem. Chem. Phys.*, 2012, **14**, 10640–10646.

162 T. Okino, A. Watanabe, H. L. Xu and K. Yamanouchi, Two-body Coulomb explosion in methylacetylene in intense laser fields: double proton migration and proton/deuteron exchange, *Phys. Chem. Chem. Phys.*, 2012, **14**, 4230–4235.

163 M. Zhang, T. Ando, A. Iwasaki, L. D. Wang, S. Koh and K. Yamanouchi, Ionization and ultrafast hydrogen migration of methylamine in few-cycle intense near-infrared laser fields, *Chem. Phys. Lett.*, 2022, **806**, 140061.

164 H. Wu, S. A. Zhang, Y. Yang, S. Z. Sun, J. Zhang, L. Deng, T. Q. Jia, Z. G. Wang and Z. R. Sun, Coulomb explosion and dissociative ionization of 1,2-dibromoethane under an intense femtosecond laser field, *RSC Adv.*, 2014, **4**, 45300–45305.

165 H. Wu, Y. Yang, S. Z. Sun, J. Zhang, L. Deng, S. A. Zhang, T. Q. Jia, Z. G. Wang and Z. R. Sun, Concerted elimination of Br_2^+ resulting from the Coulomb explosion of 1,2-dibromoethane in an intense femtosecond laser field, *Chem. Phys. Lett.*, 2014, **607**, 70–74.

166 Y. Yang, L. L. Fan, S. Z. Sun, J. Zhang, Y. T. Chen, S. A. Zhang, T. Q. Jia and Z. R. Sun, Dissociative double ionization of 1-bromo-2-chloroethane irradiated by an intense femtosecond laser field, *J. Chem. Phys.*, 2011, **135**, 064303.

167 H. Wu, Y. X. Xue, J. Q. Wen, H. Wang, L. H. Bai, W. L. He, R. J. Sun and W. L. Zheng, $BrCl^+$ elimination from Coulomb explosion of 1,2-bromochloroethane induced by intense femtosecond laser fields, *RSC Adv.*, 2019, **9**, 31853–31859.

168 J. Zhang, Y. Yang, Z. P. Li, S. A. Zhang and Z. R. Sun, Dissociative photoionization of 1,2-dichloroethane in intense near-infrared femtosecond laser field, *Chem. Phys. Lett.*, 2017, **667**, 238–243.

169 M. J. Pei, Y. Yang, J. Zhang and Z. R. Sun, Dehydrogenation involved Coulomb explosion of molecular C_2H_4FBr in an intense laser field, *Chem. Phys. Lett.*, 2018, **697**, 53–60.

170 K. Hosaka, A. Yokoyama, K. Yamanouchi and R. Itakura, Correlation between a photoelectron and a fragment ion in dissociative ionization of ethanol in intense near-infrared laser fields, *J. Chem. Phys.*, 2013, **138**, 204301.

171 K. Gope, D. M. Bittner and D. Strasser, Sequential mechanism in H_3^+ formation dynamics on the ethanol dication, *Phys. Chem. Chem. Phys.*, 2023, **25**, 6979–6986.

172 S. T. Alavi, G. A. Cooper and A. G. Suits, Coulomb explosion dynamics of methoxycarbonylsulfenyl chloride by 3D multimass imaging, *Mol. Phys.*, 2022, **120**, e1988170.

173 H. L. Xu, T. Okino, K. Nakai, K. Yamanouchi, S. Roither, X. H. Xie, D. Kartashov, L. Zhang, A. Baltuska and M. Kitzler, Two-proton migration in 1,3-butadiene in intense laser fields, *Phys. Chem. Chem. Phys.*, 2010, **12**, 12939–12942.

174 L. Zhang, S. Roither, X. H. Xie, D. Kartashov, M. Schöffler, H. L. Xu, A. Iwasaki, S. Gräfe, T. Okino, K. Yamanouchi,

A. Baltuska and M. Kitzler, Path-selective investigation of intense laser-pulse-induced fragmentation dynamics in triply charged 1,3-butadiene, *J. Phys. B: At. Mol. Phys.*, 2012, **45**, 085603.

175 K. Nagaya, K. Motomura, E. Kukk, H. Fukuzawa, S. Wada, T. Tachibana, Y. Ito, S. Mondal, T. Sakai, K. Matsunami, R. Koga, S. Ohmura, Y. Takahashi, M. Kanno, A. Rudenko, C. Nicolas, X. J. Liu, Y. Zhang, J. Chen, M. Anand, Y. H. Jiang, D.-E. Kim, K. Tono, M. Yabashi, H. Kono, C. Miron, M. Yao and K. Ueda, Ultrafast dynamics of a nucleobase analogue illuminated by a short intense X-ray free electron laser pulse, *Phys. Rev. X*, 2016, **6**, 021035.

176 A. Matsuda, M. Fushitani, R. A. Thomas, V. Zhaunerchyk and A. Hishikawa, Multiple explosion pathways of the deuterated benzene trication in 9-fs intense laser fields, *J. Phys. Chem. A*, 2009, **113**, 2254–2260.

177 U. Ablikim, C. Bomme, E. Savelyev, H. Xiong, R. Kushawaha, R. Boll, K. Amini, T. Osipov, D. Kilcoyne, A. Rudenko, N. Berrah and D. Rolles, Isomer-dependent fragmentation dynamics of inner-shell photoionized difluoroiodobenzene, *Phys. Chem. Chem. Phys.*, 2017, **19**, 13419–13431.

178 H. Wu, S. Zhang, J. Zhang, Y. Yang, L. Deng, T. Q. Jia, Z. G. Wang and Z. R. Sun, Observation of hydrogen migration in cyclohexane under an intense femtosecond laser field, *J. Phys. Chem. A*, 2015, **119**, 2052–2057.

179 H. Wu, H. Wang, Z. H. Guo and J. Q. Wen, Hydrogen migration in Coulomb explosion of cyclohexane to $C_2H_4^+$ and $C_4H_8^+$: Theoretical and experimental studies, *Int. J. Quant. Chem.*, 2018, **118**, e25764.

180 T. Endo, S. P. Neville, V. Wanie, S. Beaulieu, C. Qu, J. Deschamps, P. Lassonde, B. E. Schmidt, H. Fujise, M. Fushitani, A. Hishikawa, P. L. Houston, J. M. Bowman, M. S. Schuurmann, F. Légaré and H. Ibrahim, Capturing roaming molecular fragments in real time, *Science*, 2020, **370**, 1072–1077.

181 T. Endo, S. P. Neville, P. Lassonde, C. Qu, H. Fujise, M. Fushitani, A. Hishikawa, P. L. Houston, J. M. Bowman, F. Légaré, M. S. Schuurmann and H. Ibrahim, Electronic relaxation and dissociation dynamics in formaldehyde: pump wavelength dependence, *Phys. Chem. Chem. Phys.*, 2022, **24**, 1779–1786.

182 Y. Malakar, W. L. Pearson, M. Zohrabi, B. Kaderiya, P. K. Raju, F. Ziaee, S. Xue, A. T. Le, I. Ben-Itzhak, D. Rolles and A. Rudenko, Time-resolved imaging of bound and dissociating nuclear wave packets in strong-field ionized iodomethane, *Phys. Chem. Chem. Phys.*, 2019, **21**, 14090–14102.

183 F. Allum, N. Anders, M. Brouard, P. Bucksbaum, M. Burt, B. Downes-Ward, S. Grundmann, J. Harries, Y. Ishimura, H. Iwayama, L. Kaiser, E. Kukk, J. Lee, X. J. Liu, R. S. Minns, K. Nagaya, A. Niozu, J. Niskanen, J. O'Neal, S. Owada, J. Pickering, D. Rolles, A. Rudenko, S. Saito, K. Ueda, C. Vallance, N. Werby, J. Woodhouse, D. You, F. Ziaee, T. Driver and R. Forbes, Multi-channel photodissociation and XUV-induced charge transfer dynamics in strong-field-ionized methyl iodide studied with time-resolved recoil-frame covariance imaging, *Farad. Disc.*, 2021, **228**, 571–596.

184 M. E. Corrales, J. González-Vázquez, G. Balerdi, I. R. Solá, R. de Nalda and L. Bañares, Control of ultrafast molecular photodissociation by laser-field-induced potentials, *Nat. Chem.*, 2014, **6**, 785–790.

185 F. Allum, M. Burt, K. Amini, R. Boll, H. Kockert, P. K. Olshin, S. Bari, C. Bomme, F. Brausse, B. C. de Mirande, S. Düsterer, B. Erk, M. Geleoc, R. Geneaux, A. S. Gentleman, G. Goldsztejn, R. Guillemin, D. M. P. Holland, I. Ismail, P. Johnsson, L. Journel, J. Küpper, J. Lahl, J. W. L. Lee, S. Maclot, S. R. Mackenzie, B. Manschwetus, A. S. Mereshchenko, R. Mason, J. Palaudoux, M. N. Piancastelli, F. Penant, D. Rompotis, A. Rouzée, T. Ruchon, A. Rudenko, E. Savelyev, M. Simon, N. Schirmel, H. Stapelfeldt, S. Techert, O. Travnikova, S. Trippel, J. G. Underwood, C. Vallance, J. Wiese, F. Ziaee, M. Brouard, T. Marchenko and D. Rolles, Coulomb explosion imaging of CH_3I and CH_2ClI photodissociation dynamics, *J. Chem. Phys.*, 2018, **149**, 204313.

186 M. E. Corrales, J. González-Vázquez, R. de Nalda and L. Bañares, Coulomb explosion imaging for the visualization of a conical intersection, *J. Phys. Chem. Lett.*, 2019, **10**, 138–143.

187 F. Ziaee, K. Borne, R. Forbes, P. K. Raju, Y. Malakar, B. Kaderiya, T. Severt, I. Ben-Itzhak, A. Rudenko and D. Rolles, Single- and multi-photon-induced ultraviolet excitation and photodissociation of CH_3I probed by coincident ion momentum imaging, *Phys. Chem. Chem. Phys.*, 2023, **25**, 9999–10010.

188 K. Amini, E. Savelyev, F. Brausse, N. Berrah, C. Bomme, M. Brouard, M. Burt, L. Christensen, S. Dusterer, B. Erk, H. Höppner, T. Kierspel, F. Krecinic, A. Lauer, J. W. L. Lee, M. Müller, E. Müller, T. Mullins, H. Redlin, N. Schirmel, J. Thogersen, S. Techert, S. Toleikis, R. Treusch, S. Trippel, A. Ulmer, C. Vallance, J. Wiese, P. Johnsson, J. Küpper, A. Rudenko, A. Rouzée, H. Stapelfeldt, D. Rolles and R. Boll, Photodissociation of aligned CH_3I and $C_6H_3F_2I$ molecules probed with time-resolved Coulomb explosion imaging by site-selective extreme ultraviolet ionization, *Struct. Dynam.*, 2018, **5**, 014301.

189 M. Burt, R. Boll, J. W. L. Lee, K. Amini, H. Kockert, C. Vallance, A. S. Gentleman, S. R. Mackenzie, S. Bari, C. Bomme, S. Düsterer, B. Erk, B. Manschwetus, E. Müller, D. Rompotis, E. Savelyev, N. Schirmel, S. Techert, R. Treusch, J. Küpper, S. Trippel, J. Wiese, H. Stapelfeldt, B. C. de Miranda, R. Guillemin, I. Ismail, L. Journel, T. Marchenko, J. Palaudoux, F. Penent, M. N. Piancastelli, M. Simon, O. Travnikova, F. Brausse, G. Goldsztejn, A. Rouzée, M. Geleoc, R. Geneaux, T. Ruchon, J. Underwood, D. M. P. Holland, A. S. Mereshchenko, P. K. Olshin, P. Johnsson, S. Maclot, J. Lahl, A. Rudenko, F. Ziaee, M. Brouard and D. Rolles, Coulomb-explosion imaging of concurrent CH_2BrI photodissociation dynamics, *Phys. Rev. A*, 2017, **96**, 043415.

190 H. Kockert, J. W. L. Lee, F. Allum, K. Amini, S. Bari, C. Bomme, F. Brausse, M. Brouard, M. Burt, B. C. de Miranda, S. Düsterer, P. Eng-Johnsson, B. Erk, M. Geleoc, R. Geneaux, A. S. Gentleman, R. Guillemin, G. Goldsztejn, D. M. P. Holland, I. Ismail, L. Journel, T. Kierspel, J. Küpper, J. Lahl, S. R. Mackenzie, S. Maclot, B. Manschwetus, A. S. Mereshchenko, T. Mullins, P. K. Olshin, J. Palaudoux, F. Penent, M. N. Piancastelli, D. Rompotis, A. Rouzée, T. Ruchon, A. Rudenko, N. Schirmel, M. Simon, S. Techert, O. Travnikova, S. Trippel, C. Vallance, E. L. Wang, J. Wiese, F. Ziaee, T. Marchenko, D. Rolles and R. Boll, UV-induced dissociation of CH_2BrI probed by intense femtosecond XUV pulses, *J. Phys. B: At. Mol. Phys.*, 2022, **55**, 014001.

191 F. Allum, K. Nagaya, Y. Kumagai, J. Harries, H. Iwayama, M. Britton, P. H. Bucksbaum, M. Burt, M. Brouard, B. Downes-Ward, T. Driver, D. Heathcote, A. J. Howard, J. W. L. Lee, Y. S. Liu, E. Kukk, J. W. McManus, D. Milsesevic, A. Niozu, J. Niskanen, A. J. Orr-Ewing, S. Owada, P. A. Robertson, A. Rudenko, K. Ueda, J. Unwin, C. Vallance, T. Walmsley, R. S. Minns, D. Rolles, M. N. R. Ashfold and R. Forbes, Direct momentum imaging of charge transfer following site-selective ionization, *Phys. Rev. Lett.*, submitted.

192 F. Allum, V. Music, L. Inhester, R. Boll, B. Erk, P. Schmidt, T. M. Baumann, G. Brenner, M. Burt, P. V. Demekhin, S. Dorner, A. Ehresmann, A. Galler, P. Grychtol, D. Heathcote, D. Kargin, M. Larsson, J. W. L. Lee, Z. Li, B. Manschwetus, L. Marder, R. Mason, M. Meyer, H. Otto, C. Passow, R. Pietschnig, D. Ramm, K. Schibert, L. Schwob, R. D. Thomas, C. Vallance, I. Vidanovic, C. V. Schmising, R. Wagner, P. Walter, V. Zhaunerchyk, D. Rolles, S. Bari, M. Brouard and M. Ilchen, A localized view on molecular dissociation via electron-ion partial covariance, *Commun. Chem.*, 2022, **5**, 42.

193 X. N. Zhao, T. Xu, X. Yu, D. A. X. Ren, X. Y. Zhang, X. K. Li, P. Ma, C. C. Wang, D. D. Zhang, Q. X. Wang, X. Q. Hu, S. Z. Luo, Y. Wu, J. G. Wang and D. J. Ding, Tracking the nuclear movement of the carbonyl sulfide cation after strong-field ionization by time-resolved Coulomb-explosion imaging, *Phys. Rev. A*, 2021, **103**, 053103.

194 K. Lin, X. Q. Hu, S. Z. Pan, F. Chen, Q. Y. Ji, W. B. Zhang, H. X. Li, J. J. Qiang, F. H. Sun, X. C. Gong, H. Li, P. F. Lu, J. G. Wang, Y. Wu and J. Wu, Femtosecond resolving photodissociation dynamics of the SO_2 molecule, *J. Phys. Chem. Lett.*, 2020, **11**, 3129–3135.

195 M. L. Murillo-Sánchez, G. Reitsma, S. M. Poullain, P. Fernández-Milán, J. González-Vázquez, R. de Nalda, F. Martín, M. J. J. Vrakking, O. Kornilov and L. Bañares, Femtosecond XUV–IR induced photodynamics in the methyl iodide cation, *New J. Phys.*, 2021, **23**, 073023.

196 N. G. Kling, S. Díaz-Tendero, R. Obaid, M. R. Disla, H. Xiong, M. Sundberg, S. D. Khosravi, M. Davino, P. Drach, A. M. Carroll, T. Osipov, F. Martín and N. Berrah, Time-resolved molecular dynamics of single and double hydrogen migration in ethanol, *Nat. Commun.*, 2019, **10**, 2813.

197 D. Mishra, J. Reino-Gonzalez, R. Obaid, A. C. LaForge, S. Diaz-Tendero, F. Martín and N. Berrah, Ultrafast molecular dynamics in ionized 1-and 2-propanol: from simple fragmentation to complex isomerization and roaming mechanisms, *Phys. Chem. Chem. Phys.*, 2021, **24**, 433–443.

198 Y. H. Jiang, A. Rudenko, O. Herrwerth, L. Foucar, M. Kurka, K. U. Kühnel, M. Lezius, M. F. Kling, J. van Tilborg, A. Belkacem, K. Ueda, S. Düsterer, R. Treusch, C. Schröter, R. Moshammer and J. Ullrich, Ultrafast extreme ultraviolet induced isomerization of acetylene cations, *Phys. Rev. Lett.*, 2010, **105**, 263002.

199 Y. H. Jiang, A. Senftleben, M. Kurka, A. Rudenko, L. Foucar, O. Herrwerth, M. F. Kling, M. Leziu, J. V. Tilborg, A. Belkacem, K. Ueda, D. Rolles, R. Treusch, Y. Z. Zhang, Y. F. Liu, C. D. Schröter, J. Ullrich and R. Moshammer, Ultrafast dynamics in acetylene clocked in a femtosecond XUV stopwatch, *J. Phys. B: At. Mol. Phys.*, 2013, **46**, 164027.

200 E. L. Wang, N. G. Kling, A. C. LaForge, R. Obaid, S. Pathak, S. Bhattacharyya, S. Meister, F. Trost, H. Lindenblatt, P. Schoch, M. Kübel, T. Pfeifer, A. Rudenko, S. Díaz-Tendero, F. Martín, R. Moshammer, D. Rolles and N. Berrah, Ultrafast roaming mechanisms in ethanol probed by intense extreme ultraviolet free-electron laser radiation: electron transfer versus proton transfer, *J. Phys. Chem. Lett.*, 2023, **14**, 4372–4380.

201 F. Aguirre and S. T. Pratt, Photoionization of vibrationally hot CH_3 and CF_3, *J. Chem. Phys.*, 2005, **122**, 234303.

202 G. Hancock, A. Hutchinson, R. Peverall, G. Richmond, G. A. D. Ritchie and S. Taylor, 266 nm photolysis of CF_3I and C_2F_5I studied by diode laser gain FM spectroscopy, *Phys. Chem. Chem. Phys.*, 2007, **9**, 2234–2239.

203 D. Lin, L. Hu, S. Liu, W. K. Qi, M. Cheng, Y. K. Du and Q. H. Zhu, Resolved (v_1, v_2 = 1) combination vibrational states of CF_3 fragments in the photofragment translational spectra of CF_3I, *J. Phys. Chem. A*, 2016, **120**, 9682–9689.

204 F. Aguirre and S. T. Pratt, Velocity map imaging of the photodissociation of CF_3I^+ in the A←X band, *J. Chem. Phys.*, 2003, **119**, 9476–9485.

205 A. T. J. B. Eppink and D. H. Parker, Energy partitioning following photodissociation of methyl iodide in the A band: A velocity mapping study, *J. Chem. Phys.*, 1999, **110**, 832–844.

206 S. H. Gardiner, M. L. Lipciuc, T. N. V. Karsili, M. N. R. Ashfold and C. Vallance, Dynamics of the A-band ultraviolet photodissociation of methyl iodide and ethyl iodide via velocity-map imaging with 'universal' detection, *Phys. Chem. Chem. Phys.*, 2015, **17**, 4096–4106.

207 I. R. Solá, J. González-Vázquez, R. de Nalda and L. Bañares, Strong field laser control of photochemistry, *Phys. Chem. Chem. Phys.*, 2015, **17**, 13183–13200.

208 R. Forbes, F. Allum, S. Bari, R. Boll, K. Borne, M. Brouard, P. H. Bucksbaum, N. Ekanayake, B. Erk, A. J. Howard, P. Johnsson, J. W. L. Lee, B. Manschwetus, R. Mason, C. Passow, J. Peschel, D. E. Rivas, A. Rörig, A. Rouzée, C. Vallance, F. Ziaee, D. Rolles and M. Burt, Time-resolved

site-selective imaging of predissociation and charge transfer dynamics: the CH_3I B-band, *J. Phys. B: At. Mol. Phys.*, 2020, **53**, 224001.

209 A. Niehaus, A classical model for multiple-electron capture in slow collisions of highly charged ions with atoms, *J. Phys. B: At. Mol. Phys.*, 1986, **19**, 2925–2937.

210 L. J. Frasinski, Cumulant mapping as the basis of multi-dimensional spectrometry, *Phys. Chem. Chem. Phys.*, 2022, **24**, 20776–20787.

211 T. Zuo and A. D. Bandrauk, Charge-resonance-enhanced ionization of diatomic molecular-ions by intense lasers, *Phys. Rev. A: At., Mol., Opt. Phys.*, 1995, **52**, R2511–R2514.